Biogeosciences, 15, 5395–5413, 2018
https://doi.org/10.5194/bg-15-5395-2018

Biogeosciences
Open Access
EGU

Synthetic ozone deposition and stomatal uptake at flux tower sites

Jason A. Ducker[1], Christopher D. Holmes[1], Trevor F. Keenan[2,3], Silvano Fares[4], Allen H. Goldstein[3], Ivan Mammarella[5], J. William Munger[6], and Jordan Schnell[7]

[1]Department of Earth, Ocean, and Atmospheric Science, Florida State University, Tallahassee, Florida, USA
[2]Lawrence Berkeley National Laboratory, University of California, Berkeley, California, USA
[3]Department of Environmental Science, Policy, and Management, University of California, Berkeley, California, USA
[4]Council of Agricultural Research and Economics (CREA), Research Centre for Forestry and Wood, Arezzo, Italy
[5]Institute for Atmosphere and Earth System Research/Physics, P.O. Box 68, Faculty of Science, University of Helsinki, Finland
[6]Department of Earth and Planetary Sciences, Northwestern University, Evanston, Illinois, USA
[7]NOAA Geophysical Fluid Dynamics Laboratory, Princeton, New Jersey, USA

Correspondence: Jason A. Ducker (jad10d@my.fsu.edu)

Received: 6 April 2018 – Discussion started: 18 April 2018
Revised: 8 August 2018 – Accepted: 22 August 2018 – Published: 6 September 2018

Abstract. We develop and evaluate a method to estimate O_3 deposition and stomatal O_3 uptake across networks of eddy covariance flux tower sites where O_3 concentrations and O_3 fluxes have not been measured. The method combines standard micrometeorological flux measurements, which constrain O_3 deposition velocity and stomatal conductance, with a gridded dataset of observed surface O_3 concentrations. Measurement errors are propagated through all calculations to quantify O_3 flux uncertainties. We evaluate the method at three sites with O_3 flux measurements: Harvard Forest, Blodgett Forest, and Hyytiälä Forest. The method reproduces 83 % or more of the variability in daily stomatal uptake at these sites with modest mean bias (21 % or less). At least 95 % of daily average values agree with measurements within a factor of 2 and, according to the error analysis, the residual differences from measured O_3 fluxes are consistent with the uncertainty in the underlying measurements.

The product, called synthetic O_3 flux or SynFlux, includes 43 FLUXNET sites in the United States and 60 sites in Europe, totaling 926 site years of data. This dataset, which is now public, dramatically expands the number and types of sites where O_3 fluxes can be used for ecosystem impact studies and evaluation of air quality and climate models. Across these sites, the mean stomatal conductance and O_3 deposition velocity is 0.03–1.0 cm s^{-1}. The stomatal O_3 flux during the growing season (typically April–September) is 0.5–11.0 nmol O_3 m^{-2} s^{-1} with a mean of 4.5 nmol O_3 m^{-2} s^{-1} and the largest fluxes generally occur where stomatal conductance is high, rather than where O_3 concentrations are high. The conductance differences across sites can be explained by atmospheric humidity, soil moisture, vegetation type, irrigation, and land management. These stomatal fluxes suggest that ambient O_3 degrades biomass production and CO_2 sequestration by 20 %–24 % at crop sites, 6 %–29 % at deciduous broadleaf forests, and 4 %–20 % at evergreen needleleaf forests in the United States and Europe.

1 Introduction

Surface ozone (O_3) is toxic to both people and plants. Present-day and recent historical O_3 levels reduce carbon sequestration in the biosphere (Reich and Lassoie, 1984; Guidi et al., 2001; Sitch et al., 2007; Ainsworth et al., 2012), perturb the terrestrial water cycle (Lombardozzi et al., 2012, 2015), and cause around $ 25 billion in annual crop losses (Reich and Amundson, 1985; Van Dingenen et al., 2009; Avnery et al., 2011; Tai et al., 2014). The basic plant responses to O_3 injury are well established from controlled exposure experiments (e.g., Wittig et al., 2009; Ainsworth et al., 2005, 2012; Hoshika et al., 2015), but few datasets are available to quantify O_3 fluxes and responses for whole ecosys-

tems or plant functional types that are represented within regional and global biosphere and climate models. The eddy covariance method has been widely used to measure land–atmosphere fluxes of carbon, water, and energy and evaluate their representation in models (Baldocchi et al., 2001; Bonan et al., 2011), but few towers measure O_3 fluxes (Munger et al., 1996; Fowler et al., 2001; Keronen et al., 2003; Gerosa et al., 2004; Lamaud et al., 2009; Fares et al., 2010; Stella et al., 2013; Zona et al., 2014). A recent review identified just 78 field measurements of O_3 fluxes over vegetation during the last 4 decades, many lasting just a few weeks (Silva and Heald, 2018). This paper demonstrates a reliable method to estimate O_3 fluxes at 103 eddy covariance flux towers spanning over 2 decades to enable O_3 impact studies on ecosystem scales.

The land surface is a terminal sink for atmospheric O_3 due to the reactivity of O_3 with unsaturated organic molecules and the modest solubility of O_3 in water. Surface deposition is 20 % of the total loss in tropospheric O_3, making it an important control on air pollution (Wu et al., 2007; Young et al., 2013; Kavassalis and Murphy, 2017). This O_3 deposition flux includes stomatal uptake into leaves, where O_3 can cause internal oxidative damage, and less harmful non-stomatal deposition to plant cuticles, stems, bark, soil, and standing water (Fuhrer, 2000; Zhang et al., 2002; Ainsworth et al., 2012). O_3 can also react with biogenic volatile organic compounds, particularly terpenoid compounds, in the plant canopy air, and this process is commonly included in non-stomatal deposition (Kurpius and Goldstein, 2003). The deposition flux (mol O_3 m^{-2} s^{-1}) can be described as

$$F_{O_3} = v_d n\,(\chi - \chi_0) = v_d n \chi, \quad (1)$$

where χ and χ_0 are the O_3 mole fractions (mol mol^{-1}) in the atmosphere and at the surface, respectively, n is the molar density of air (mol m^{-3}), and v_d is a deposition velocity (m s^{-1}) that expresses the net vertical O_3 transport between the height where χ is measured and the surface. F_{O_3} is defined positive for flux towards the ground. Equation (1) reasonably assumes that $\chi_0 = 0$ because terrestrial surfaces have abundant organic compounds that react with and destroy O_3. The deposition velocity can be decomposed into resistances (s m^{-1}) for aerodynamic transport (r_a), diffusion in the quasi-laminar layer (r_b), stomatal uptake (r_s), and non-stomatal deposition (r_{ns}) (Wesely, 1989):

$$v_d^{-1} = r_a + r_b + \left(r_s^{-1} + r_{ns}^{-1}\right)^{-1}. \quad (2)$$

For stomatal and non-stomatal processes, the rates are often expressed as conductances (m s^{-1}), which are the inverse of the resistances: $g_s = r_s^{-1}$ and $g_{ns} = r_{ns}^{-1}$. The sum of stomatal and non-stomatal conductances is the vegetation canopy conductance, $g_c = g_s + g_{ns}$. The stomatal O_3 flux is the portion of F_{O_3} that enters the stomata, and can be described as

$$F_{s,O_3} = F_{O_3} g_s (g_s + g_{ns})^{-1} = v_d n \chi g_s (g_s + g_{ns})^{-1}. \quad (3)$$

To construct the synthetic O_3 flux, or SynFlux, we use measurements of O_3 concentration and standard eddy covariance flux measurements to derive nearly all of the terms in Eqs. (1)–(3) from surface observations, using some additional information from remote sensing and models. This enables the estimation of F_{O_3} and F_{s,O_3}, as described in Sect. 2. Section 3 evaluates the method against observations at three sites that measure F_{O_3} and examines the importance of stomatal and non-stomatal deposition. Section 4 uses SynFlux to assess the spatial patterns of O_3 uptake to vegetation and to compare flux-based metrics of O_3 damage with concentration-based metrics. Finally, we discuss the strengths, limitations, and implications of our approach in Sect. 5.

2 Data sources and methods

2.1 SynFlux: synthetic O_3 flux

The FLUXNET2015 dataset (Pastorello et al., 2017) aggregates measurements of land–atmosphere fluxes of CO_2, H_2O, momentum, and heat at sites around the world (http://fluxnet.fluxdata.org/data/fluxnet2015-dataset; last access: 24 February 2017). Measurements are made with the eddy covariance method on towers above vegetation canopies (Baldocchi et al., 2001; Anderson et al., 1984; Goldstein et al., 2000) with consistent gap filling (Reichstein et al., 2005; Vuichard and Papale, 2015) and quality control across sites (Pastorello et al., 2014). Flux and meteorological quantities are reported in half-hour intervals. We analyze data from all sites in the United States and Europe in the FLUXNET2015 Tier 1 dataset. This analysis is restricted to the US and Europe because these regions have dense O_3 monitoring networks, described below. There are 103 sites meeting these criteria, all listed in Table S1 in the Supplement with references to full site descriptions. Three of these sites – Blodgett Forest, Harvard Forest, and Hyytiälä Forest – measure O_3 flux with the eddy covariance method, which we will use in Sect. 3 to evaluate our methods.

SynFlux aims to constrain O_3 deposition and stomatal uptake as much as possible from measured water, heat, and momentum fluxes, in contrast to other methods (Finkelstein et al., 2000; Mills et al. 2011; Schwede et al., 2011; Yue et al., 2014) that rely more heavily on atmospheric models or parameterizations of stomatal conductance. From the eddy covariance measurements, we derive the resistance components of Eq. (2) using methods similar to past studies (Kurpius and Goldstein, 2003; Gerosa et al., 2005; Fares et al., 2010). The aerodynamic and quasi-laminar layer resistances (r_a and r_b, respectively) are derived from measured wind speed, friction velocity, and fluxes of sensible and latent heat every half hour using Monin–Obukhov similarity theory (Foken, 2017). The stomatal conductance for O_3 (g_s) is derived from the measured water vapor flux and meteorological data every half

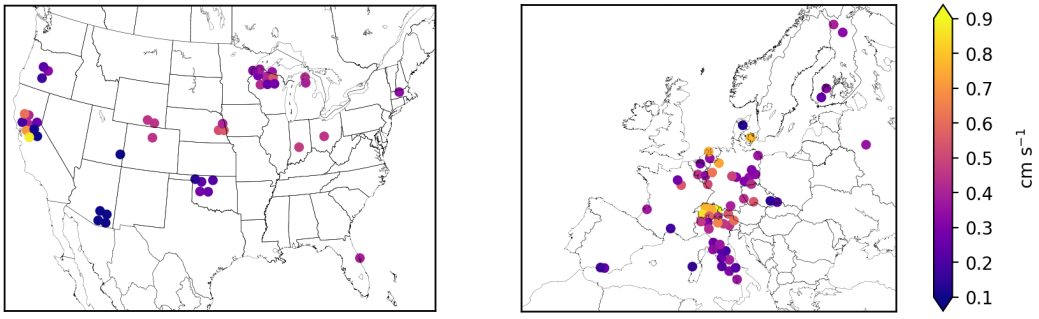

Figure 1. Mean stomatal conductance for O_3 (g_s) during daytime in the growing season at FLUXNET2015 sites in the United States and Europe. Symbols of some sites have been moved slightly to reduce overlap and improve legibility.

hour with the inverted Penman–Monteith equation (Monteith, 1981; Gerosa et al., 2007). Supplement S1 provides further details of the resistance and conductance calculations. Some studies instead calculate g_s from gross primary productivity (Lamaud et al., 2009; El-Madany et al., 2017), but that method is less widely used than the Penman–Monteith approach adopted here. The Penman–Monteith method of calculating stomatal conductance has been successfully applied across FLUXNET sites previously (Medlyn et al., 2017; Novick et al., 2016; Knauer et al., 2017; Lin et al., 2018). Those studies and others caution that, since evapotranspiration measurements include evaporation from ground, the stomatal conductance could be overestimated. While there are methods for quantifying and removing the evaporative fraction of evapotranspiration from eddy covariance data (Wang et al., 2014; Zhou et al., 2016; Scott and Biederman, 2017), a more common approach is to restrict analysis to conditions when transpiration dominates. We follow this second approach, analyzing only daytime data during the growing season, and use filtering criteria similar to Knauer et al. (2017). We define daytime as Sun elevation angle above 4° and the growing season as days when gross primary productivity (GPP) exceeds 20 % of the annual maxima in GPP. To avoid complications to the Penman–Monteith equation from wet canopies, we exclude times when dew may be present (RH > 80 %), and days with precipitation (> 5 mm). We also exclude the top and bottom 1 % of g_s values, which include many unrealistic outliers (e.g., $|g_s| > 0.5\,\mathrm{m\,s^{-1}}$). Figure 1 shows the mean stomatal conductance during the growing season at all sites.

The terms in Eqs. (1)–(3) that cannot be derived from FLUXNET2015 measurements are O_3 mole fraction and non-stomatal conductance. The O_3 mole fraction is taken from a gridded dataset of hourly O_3 measurements that spans the contiguous United States and Europe (Schnell et al., 2014). This dataset has 1° spatial resolution, so some differences from measured O_3 abundances at individual sites are inevitable. Schnell et al. (2014) estimated these errors to be 6–9 ppb (rms) or about 15 % of summer mean O_3 in the US and similar in Europe. Figure 2 shows that the daytime gridded O_3 concentrations correlate well with observations at three flux tower sites where O_3 was measured ($R^2 = 0.63$–0.87) and have modest negative bias (5–10 ppb, −12 % to −28 %), consistent with the accuracy reported by Schnell et al. (2014). We use the Zhang et al. (2003) parameterization of non-stomatal conductance, which accounts for O_3 deposition to leaf cuticles and ground and was developed from measurements in the eastern United States. The parameterization requires leaf-area index, which we take from satellite remote sensing (Claverie et al., 2014, 2016), snow depth, which we take from MERRA2 reanalysis (GMAO, 2015; Gelaro et al., 2017), and standard meteorological data provided by FLUXNET2015. Uncertainties in these variables are described in Sect. 2.4. Performance of the non-stomatal parameterization is examined in Sect. 3.2.

Figure 3 shows the stomatal O_3 flux at each site calculated with Eq. (3), and then averaged over the growing season. Figure S1 shows the corresponding total O_3 flux (Eq. 1). We refer to these products as the "synthetic" total O_3 flux ($F_{O_3}^{syn}$) and synthetic stomatal O_3 flux (F_{s,O_3}^{syn}). Superscript "syn" distinguishes these synthetic quantities from the $F_{O_3} F_{s,O_3}$ observed total O_3 flux ($F_{O_3}^{obs}$) and observation-derived stomatal O_3 flux (F_{s,O_3}^{obs}), which are only available at a few sites. Together, we refer to $F_{O_3}^{syn}$ and F_{s,O_3}^{syn} as SynFlux. In total, the measurements required to calculate F_{s,O_3}^{syn} are O_3 mole fraction, sensible and latent heat fluxes, friction velocity, temperature, pressure, humidity, canopy height, and leaf-area index. There are 43 sites in the US and 60 sites in Europe within the FLUXNET Tier 1 database with sufficient measurements to calculate F_{s,O_3}^{syn}.

2.2 Observed O_3 flux

We evaluate SynFlux and its inputs at three sites where O_3 flux measurements are available: Harvard Forest, Massachusetts, United States (Munger et al., 1996); Blodgett Forest, California, United States (Fares et al., 2010); and Hyytiälä Forest, Finland (Keronen et al., 2003; Mammarella

Table 1. Description of sites that measure O_3 flux and their daytime growing season conditions*.

	Blodgett Forest, California, USA	Hyytiälä Forest, Finland	Harvard Forest, Massachusetts, USA
Latitude, longitude	38.8953, −120.6328	61.8475, 24.2950	42.5378, −72.1715
Plant functional type	Evergreen needleleaf	Evergreen needleleaf	Deciduous broadleaf
Years of data	2001–2007	2007–2012	1993–1999
Days of observations	1281	1098	1281
Canopy height (m)	8	15	24
GPP (μmol m^{-2} s^{-1})	9.22 ± 3.55	11.1 ± 5.02	12.4 ± 7.62
ET (mmol m^{-2} s^{-1})	3.25 ± 1.23	1.71 ± 0.82	2.95 ± 1.70
PAR (μmol m^{-2} s^{-1})	875 ± 149	690 ± 203	876 ± 222
Air temperature (°C)	19.1 ± 5.36	13.3 ± 5.99	17.65 ± 5.75
VPD (kPa)	1.51 ± 0.61	0.73 ± 0.32	0.90 ± 0.34
O_3 (ppb)	55.4 ± 13.4	32.2 ± 8.68	48.8 ± 15.8
F_{s,O_3} (nmol O_3 m^{-2} s^{-1})	5.18 ± 2.11	4.35 ± 1.66	7.23 ± 4.87
Precipitation (mm d^{-1})	0.09 ± 0.49	0.42 ± 0.89	0.28 ± 0.82

* Values are mean ± standard deviation of daily averages, using daytime observations only. GPP is gross primary productivity. ET is evapotranspiration. PAR is photosynthetically active radiation. VPD is vapor pressure deficit. F_{s,O_3} is observation-derived stomatal O_3 flux.

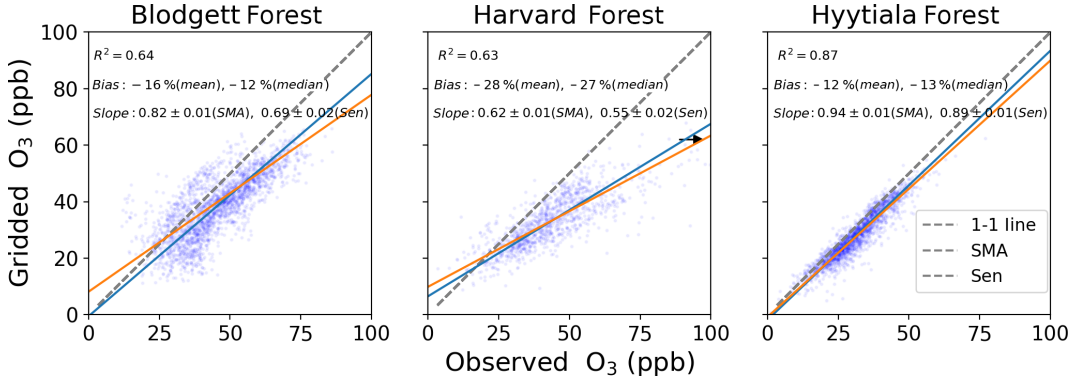

Figure 2. Gridded and observed daily daytime O_3 concentrations at Blodgett, Harvard, and Hyytiälä forests. Inset numbers provide the coefficient of determination (R^2), mean and median bias, the standard major axis (SMA) slope, the Thiel–Sen (Sen) slope, and the 68 % confidence interval of the slopes. The black arrow points towards outliers that are not shown.

et al., 2007; Rannik et al., 2009). These forest sites sample a range of environmental and ecosystem conditions summarized in Table 1. All three sites have at least 6 years of half-hourly or hourly flux measurements. Two sites are evergreen needleleaf forests (Blodgett and Hyytiälä), while one is a deciduous broadleaf forest containing some scattered stands of evergreen needleleaf trees (Harvard). Climate also differs across these sites. Blodgett Forest has a Mediterranean climate with cool, wet winters and hot, dry summers. Hyytiälä and Harvard forests have cold winters and wetter summers, with Harvard Forest being the warmer of the two.

Harvard Forest water vapor flux measurements were recalibrated for this work based on matching water vapor mixing ratio measured by the flux sensor to levels calculated from ambient relative humidity and air temperature, resulting in a 30 % increase in evapotranspiration during the 1990s and no change since 2006. In addition, we remove sub-canopy evaporation from the measured water vapor flux before the Penman–Monteith calculation. Based on past measurements at these sites, the sub-canopy fraction of evapotranspiration is 20 % at Hyytiälä Forest and 10 % at Harvard Forest in summer (Moore et al., 1996; Launiainen et al., 2005). We are unable to make this correction at all FLUXNET sites since water vapor flux is typically measured only above canopy.

At these three sites, observation-derived v_d, g_{ns}, and F_{s,O_3} can be derived from the F_{O_3} measurements with methods that differ slightly from Sect. 2.1. O_3 deposition velocity is inferred from measurements of O_3 concentration and flux via $v_d = F_{O_3}(n\chi)^{-1}$. Resistance or conductance terms r_a, r_b, and g_s are calculated as described in Sect. 2.1, and then both canopy and non-stomatal conductance are derived from observations via $g_c = \left(v_d^{-1} - r_a - r_b\right)^{-1}$ and $g_{ns} = g_c - g_s$, respectively. With those values, Eq. (3) gives the observation-

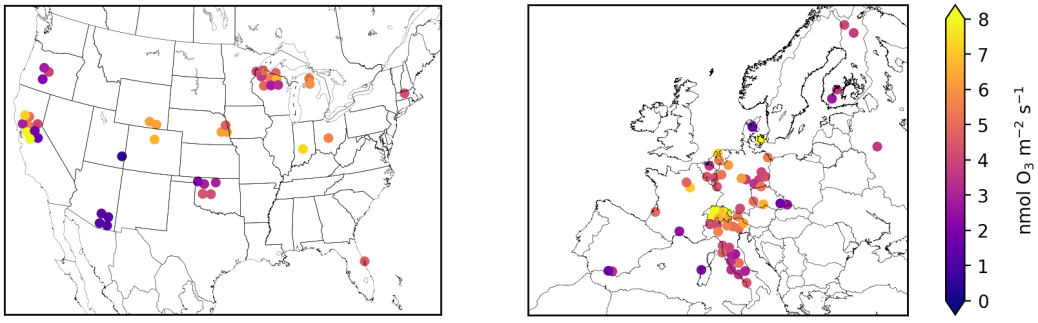

Figure 3. Mean synthetic stomatal O_3 flux (F^{syn}_{s,O_3}, Sect. 2.1) during the daytime growing season at FLUXNET2015 sites in the United States and Europe. Symbols of some sites have been moved slightly to reduce overlap and improve legibility.

derived stomatal O_3 flux. Synthetic and observation-derived stomatal O_3 fluxes are both calculated with Eq. (3) and use the same observation-derived g_s, r_a, and r_b but different values of g_{ns}, v_d, and O_3 mole fraction.

2.3 Gap filling for friction velocity

The FLUXNET2015 dataset uses gap filling for most flux and meteorological measurements (Vuichard and Papale, 2015), but not for friction velocity (u_*), which is required to calculate v_d and F^{syn}_{s,O_3}. Filling this one variable would significantly reduce the fraction of missing data in our analysis. Monin–Obukhov similarity theory predicts that friction velocity will be proportional to wind speed in the surface layer, for a given roughness length and stability regime (Foken, 2017). On this basis, we regress the available friction velocity measurements against wind speed and net radiation (a proxy for stability) separately for each site and month (a proxy for vegetation roughness). This gap filling was possible at 91 sites that report net radiation measurements.

The predicted friction velocities from the regression model are correlated with available observations ($R^2 > 0.5$) and have minimal mean bias (±10 %) at 85 out of 91 eligible sites (Fig. S3 in the Supplement), with most sites (63 out of 91) showing strong correlations ($R^2 > 0.7$). At the remaining six sites with lower regression model performance ($R^2 < 0.5$) we do not use u_* gap filling. The u_* gap filling increases the number of F^{syn}_{s,O_3} estimates by 1 %–20 %. Time periods with u_* gaps have no significant bias in meteorological conditions (e.g., mean wind speed, radiation, energy fluxes) compared to periods with u_* measurements. As a result, the differences in monthly mean F^{syn}_{s,O_3} with and without gap filling are small (10 % rms). So, although the u_* gap filling is a potential source of uncertainty, the F^{syn}_{s,O_3} estimates are robust. The following analysis will use the gap-filled data, but our results do not change in any meaningful way if we use the unfilled data.

2.4 Error analysis, averaging, and numerical methods

We quantify the errors in $F^{syn}_{O_3}$, F^{syn}_{s,O_3}, and all other calculated variables from the measurement uncertainties using standard techniques for propagation of errors through all equations (see Supplement S2). This method provides the uncertainty, quantified as the standard deviation, of each variable in each half-hour interval. The error analysis reveals that F^{syn}_{s,O_3} and other derived quantities have uncertainties that change from hour to hour by 2 orders of magnitude (Fig. S2). In addition, many extreme values of F^{syn}_{s,O_3}, g_s, and other variables have very large uncertainties. We retain these outliers in our analysis and use the error analysis to appropriately reduce their influence on averages and other statistics, as described below, without discarding data.

The FLUXNET2015 dataset contains error estimates for sensible and latent heat measurements. We use these reported values in the error analysis. Where uncertainties in these fluxes are missing, we fill the gaps using a linear regression of available flux errors against flux values for that site. For friction velocity, the uncertainty is the prediction error in the linear model used for gap filling (Sect. 2.3). Based on expert judgment, the standard deviation of O_3 mole fraction is set to 20 %, pressure to 0.5 hPa, temperature to 0.5 K, relative humidity to 5 %, and canopy height to the lesser of 15 % or 2 m. For remotely sensed leaf-area index, the uncertainty is 1.1 $m^2\ m^{-2}$ for all vegetation types (Claverie et al., 2013, 2016). Snow depth uncertainty in MERRA2 is 0.08 m (Reichle et al., 2017). The Zhang et al. (2003) g_{ns} parameterization has five vegetation-specific parameters and all are assigned 50 % standard deviation. Zero error is assumed for the flux tower height. Based on these inputs, the median relative uncertainty in F^{syn}_{s,O_3} is 44 %, but it rises to several hundred percent for some half-hour intervals. The error analysis shows that most of the uncertainty in F^{syn}_{s,O_3} derives from uncertainty in the latent heat flux measurement.

Daily and monthly averages of F^{syn}_{s,O_3} and other quantities are constructed in stages. We first calculate a mean diurnal cycle for the day or month by pooling measurements during

each hour in a maximum likelihood estimate, a weighted average that accounts for the uncertainty in each measurement. The maximum likelihood estimate is appropriate when combining values from the same distribution, which is expected to apply for measurements within a particular hour, but not across hours of the day. We then average across hours with an unweighted mean to calculate the daily or monthly value. For the daily averages, there are one to two observations within each hour. For the monthly averages, there are typically 30 to 60 in each hour of the day. We calculate seasonal averages with an unweighted mean of monthly values. Uncertainties are propagated through each stage of these averages, as detailed in Supplement S2. We compared averages with and without uncertainty weighting. The uncertainty-weighted averages tend to be smaller and less variable than unweighted averages because the error propagation identifies when outliers and large values have greater uncertainty. For example, the monthly values of g_c derived from observations at Harvard Forest are $0.57 \pm 0.11\,\mathrm{cm\,s^{-1}}$ with uncertainty weighting and $0.68 \pm 0.17\,\mathrm{cm\,s^{-1}}$ without. Our discussion focuses on uncertainty-weighted daily averages of daytime data.

Analyses are performed in Python 3.5 with NumPy, Pandas, PySolar, and Statsmodels (Reda and Andreas, 2005; Van Der Walt et al., 2006; McKinney, 2010; Seabold et al., 2010). We quantify linear relationships between variables using the coefficient of determination (R^2), a parametric slope estimator (standard major axis or SMA, Warton et al., 2006) and a non-parametric slope estimator (Thiel–Sen slope, Sen, 1968), which is more robust against outliers.

2.5 Data availability

The SynFlux dataset produced in this work is available at https://doi.org/10.5281/zenodo.1402054 (last access: 30 August 2018). The dataset includes synthetic stomatal and total O_3 fluxes, O_3 concentrations, O_3 deposition velocity, canopy conductance, stomatal conductance, and all of their propagated uncertainties. Monthly mean values are provided with and without u_* gap filling, for 103 sites totaling 926 site years.

3 SynFlux evaluation

3.1 Evaluation of synthetic fluxes

Figure 4 compares daily daytime averages of synthetic $F^{\mathrm{syn}}_{\mathrm{s,O_3}}$ to $F_{\mathrm{s,O_3}}$ observation-derived $F^{\mathrm{obs}}_{\mathrm{s,O_3}}$. $F^{\mathrm{syn}}_{\mathrm{s,O_3}}$ and $F^{\mathrm{obs}}_{\mathrm{s,O_3}}$ are calculated from the same observation-derived stomatal conductance (g_s) and aerodynamic resistances (r_a and r_b), but differ in the O_3 mole fraction and non-stomatal conductance (g_{ns}) that they use (see Sects. 2.1 and 2.2). At all three sites, $F^{\mathrm{syn}}_{\mathrm{s,O_3}}$ is strongly correlated with measured values ($R^2 = 0.83$–0.93). The mean and median biases are $-16\,\%$ to $-21\,\%$ and at least 95 % of $F^{\mathrm{syn}}_{\mathrm{s,O_3}}$ values agree with measurements within a factor of 2. The majority of $F^{\mathrm{syn}}_{\mathrm{s,O_3}}$ values lie near the 1 : 1 line with $F^{\mathrm{obs}}_{\mathrm{s,O_3}}$ and the slopes (0.71 to 0.85) reflect this. The half-hourly or hourly measured and synthetic fluxes still have some outliers (Fig. S2), but the error analysis reveals that many of the outlying points have large uncertainties. For 98 % of points, the differences between $F^{\mathrm{syn}}_{\mathrm{s,O_3}}$ and $F^{\mathrm{obs}}_{\mathrm{s,O_3}}$ are less than the 95 % confidence interval derived from the error analysis (two-sided t-test). Thus, the errors in $F^{\mathrm{syn}}_{\mathrm{s,O_3}}$ are consistent with the propagated uncertainty in the observations. The half-hourly $F^{\mathrm{syn}}_{\mathrm{s,O_3}}$ values perform similarly well against observations (Fig. S4), but our analysis focuses on averages. The performance of daily $F^{\mathrm{syn}}_{\mathrm{s,O_3}}$ is partially due to resolving the seasonal cycle. If we subtract the mean seasonal cycle from both synthetic and observation-derived daily $F_{\mathrm{s,O_3}}$, the residual correlation is $R^2 = 0.5$–0.7 (vs. 0.9 with the seasonal cycle included). This represents the skill of SynFlux at reproducing within-month and interannual variability. Overall, these results suggest that synthetic $F^{\mathrm{syn}}_{\mathrm{s,O_3}}$ is a reliable estimate of stomatal O_3 uptake into plants that can be used at flux tower sites without O_3 measurements.

The measurements also enable us to evaluate synthetic total deposition, $F^{\mathrm{syn}}_{\mathrm{O_3}}$, and synthetic O_3 deposition velocity, $v^{\mathrm{syn}}_{\mathrm{d}}$, although these are less relevant to ecosystem impacts than stomatal uptake, $F^{\mathrm{syn}}_{\mathrm{s,O_3}}$. For daily averages, Fig. S5 shows that $F^{\mathrm{syn}}_{\mathrm{O_3}}$ bias ($-13\,\%$ to $+65\,\%$), slope (0.3–1.4), and R^2 (0.05–0.43) are all worse than for $F^{\mathrm{syn}}_{\mathrm{s,O_3}}$. The daily $v^{\mathrm{syn}}_{\mathrm{d}}$ performance is similar (Fig. S6, bias: $-26\,\%$ to $+41\,\%$, slope: 0.3–1.1, R^2: 0.16–0.37). Monthly averages of $v^{\mathrm{syn}}_{\mathrm{d}}$ and $F^{\mathrm{syn}}_{\mathrm{O_3}}$ both improve the correlation with observations ($R^2 \sim 0.12$–0.54). The reasons for the better performance of $F^{\mathrm{syn}}_{\mathrm{s,O_3}}$ compared to $F^{\mathrm{syn}}_{\mathrm{O_3}}$ can be derived from Eq. (3). The canopy resistance for O_3 is normally much greater than the quasi-laminar layer and aerodynamic resistances, meaning $r_c \gg r_a$ and $r_c \gg r_b$, often by a factor of 3–10. Therefore, the O_3 deposition velocity is approximately $v_d \approx r_c^{-1} = g_c$. Under these conditions, Eq. (1) simplifies to $F_{O_3} \approx n\chi(g_s + g_{ns})$ and Eq. (3) simplifies to $F_{s,O_3} \approx n\chi g_s$. While g_s is calculated from measured H_2O fluxes, g_{ns} comes from a parameterization, which inevitably introduces error into g_{ns} and $F^{\mathrm{syn}}_{\mathrm{O_3}}$. However, $F^{\mathrm{syn}}_{\mathrm{s,O_3}}$ has little sensitivity to g_{ns} regardless of whether stomatal or non-stomatal conductance is larger. We confirm this insensitivity in tests where the parameterized g_{ns} value is doubled at 10 sites. The hourly $F^{\mathrm{syn}}_{\mathrm{s,O_3}}$ values change only 3 %–8 %. Since $F^{\mathrm{syn}}_{\mathrm{s,O_3}}$ has little sensitivity to g_{ns} or its errors, it can be calculated more accurately than $F^{\mathrm{syn}}_{\mathrm{O_3}}$, as seen when comparing Figs. 4 and S4. Despite its larger errors, the means of $F^{\mathrm{syn}}_{\mathrm{O_3}}$ and $v^{\mathrm{syn}}_{\mathrm{d}}$ are within 50 % of the observed value at two sites and within a factor of 2 at all, which may be useful for some applications, given the scarcity of prior F_{O_3} measurements and observation-derived estimates of v_d.

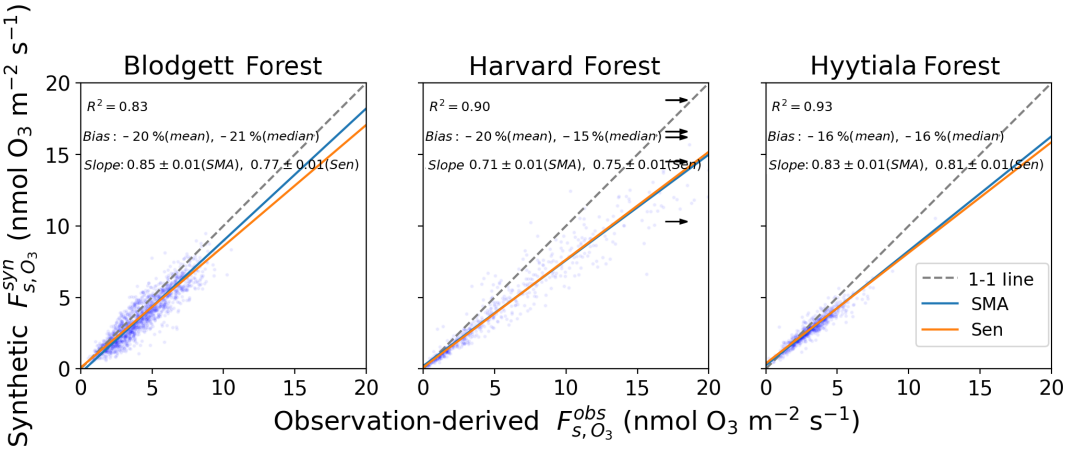

Figure 4. Synthetic and observation-derived daily daytime stomatal O_3 flux. See Sect. 2.1 for a definition of F^{syn}_{s,O_3} and Fig. 2 for an explanation of the lines and inset text.

3.2 Stomatal and non-stomatal deposition

Figure 5 shows the seasonal cycles of observation-derived O_3 deposition velocity and its important components at the three study sites with O_3 flux measurements. For low or moderately reactive gases like O_3, canopy resistance is typically greater than aerodynamic or quasi-laminar layer resistance, so it controls the overall deposition velocity. At these three sites, deposition velocity is lowest in winter (0.1–0.2 cm s^{-1}) and highest in summer (0.5–0.6 cm s^{-1}). Stomatal conductance peaks during warm and wet months, which explains most of this seasonal variation, except at Blodgett Forest as discussed below. Traditionally, stomatal conductance was thought to exceed non-stomatal conductance during the growing season at most vegetated sites (Wesely, 1989; Zhang et al., 2003), although this has been challenged more recently (Altimir et al., 2006; Stella et al., 2011a; Wolfe et al., 2011; Plake et al., 2015). At both Harvard and Hyytiälä forests, the mean stomatal conductance (0.2–0.6 cm s^{-1}) is 1.5–6 times larger than non-stomatal conductance (0.08–0.2 cm s^{-1}) during the growing season, so about 60 %–90 % of O_3 deposition occurs through stomatal uptake. At Blodgett, non-stomatal conductance slightly exceeds stomatal conductance in summer (0.4 vs. 0.3 cm s^{-1}). The fast non-stomatal deposition is explained by O_3 reacting with biogenic terpenoid emissions below the flux measurement height (Kurpius and Goldstein, 2003; Fares et al., 2010). As documented in past work, these biogenic emissions depend strongly on temperature and light and have a large seasonal cycle with maxima in summer and minima in winter, so stomatal uptake is generally < 50 % of O_3 deposition at Blodgett in the summer but > 70 % in winter (Kurpuis and Goldstein, 2003; Fares et al., 2010; Wolfe et al. 2011).

A recent analysis of O_3 flux measurements at Harvard Forest suggests that non-stomatal deposition averages 40 % of daytime O_3 deposition during summer months, with a range of 20 %–60 % across years (Clifton et al., 2017). Our analysis of the same site does not support such a large role for non-stomatal deposition at this site in summer. For each year, we calculate summer daytime means of g_s and g_c by averaging the June–September values, and then calculate the non-stomatal fraction of deposition $(1 - g_s/g_c)$. Averaged across years 1993–2000, we find that 8 % of daytime O_3 deposition is non-stomatal during the summer, with a range of −33 % to 34 % across years. Negative fractions mean that stomatal conductance is large enough to explain all O_3 deposition. A large negative non-stomatal fraction (−33 %) occurs in only one year (1996) and no other year is less than −11 %, which is within uncertainty of 0 % (2σ) according to the error propagation. Despite the small or zero non-stomatal fraction found here, our results continue to support the large year-to-year variability of this fraction reported by Clifton et al. (2017). The re-calibrated latent heat flux measurements are the main reason that our results differ from prior work and Supplement S3 provides further details. At Hyytiälä Forest, our results are consistent with prior work that found that the non-stomatal deposition is 26 % to 44 % of daytime O_3 deposition during the growing season (Rannik et al., 2012). Nevertheless, non-stomatal deposition equals or exceeds stomatal uptake where there are large terpene emissions (e.g., Blodgett) and at some other temperate sites that probably lack large biogenic emissions (Fowler et al., 2001; Cieslik, 2004; Lamaud et al., 2009; Stella et al., 2011b; El-Madany et al., 2017). We also examined interannual variation in O_3 deposition velocity. We find that the mean summer daytime v_d is 0.40–0.68 cm s^{-1} at Harvard Forest, 0.42–0.65 cm s^{-1} at Blodgett Forest, and 0.43–0.51 cm s^{-1} at Hyytiälä. This range for Harvard Forest is somewhat smaller than other recent work (0.5–1.2 cm s^{-1}; Clifton et al., 2017) because of the uncertainty-weighted averages used here (Sect. 2.4).

The data here also provide an opportunity to evaluate the parameterization of g_{ns} non-stomatal conductance (Zhang

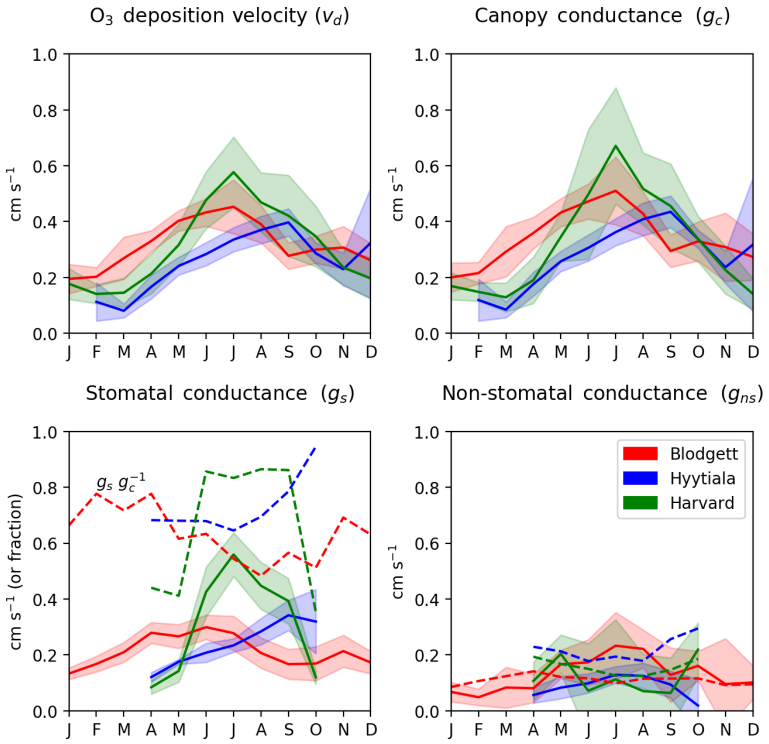

Figure 5. Observed O_3 deposition velocity and its in-canopy components at sites with O_3 flux measurements. Lines show the multi-year mean and multi-year standard deviation calculated from the monthly averages described in Sect. 2.4. Dashed lines in the stomatal conductance panel show the stomatal fraction of total canopy conductance ($g_s\, g_c^{-1}$) and dashed lines in the non-stomatal conductance panel show the parameterized g_{ns} value.

et al., 2003). The parameterized g_{ns} has a similar mean to observation-derived values in summer at Harvard Forest (0.16 vs. 0.12 cm s^{-1}) and Hyytiälä (0.15 vs. 0.25 cm s^{-1}). At Blodgett Forest, the parameterized g_{ns} is about half of observation-derived g_{ns} in summer, but this is not surprising since the parameterization does not account for O_3 reactions with biogenic volatile organic compounds (BVOCs), which are known to be important at this site (Fares et al., 2010). In winter, however, the parameterized g_{ns} values at Blodgett Forest are similar to observations (0.10 vs. 0.08 cm s^{-1}). The parameterization is therefore able to roughly predict mean non-stomatal conductance in the absence of major BVOC emissions. Nevertheless, the parameterization reproduces almost none of the daily variability of g_{ns} at any site ($R^2 < 0.1$, Fig. S7). This corroborates the recent field assessment that non-stomatal conductance is a weak point of most current dry deposition algorithms (Wu et al., 2018). We attempted, unsuccessfully, to use BVOC emissions from the MEGAN biogenic emission model (Guenther et al., 2012) to improve the g_{ns} parameterization, but the correlations between compounds that react fastest with O_3 (monoterpenes and sesquiterpenes) and the observation-derived daily mean g_{ns} were poor ($R^2 \leq 0.15$). On that basis, $F_{O_3}^{syn}$ may also underestimate total O_3 deposition at other sites with high monoterpene and sesquiterpene emissions, such as warm-weather pine forests, but F_{s,O_3}^{syn} should retain its quality everywhere.

4 SynFlux applications

4.1 Spatial patterns of synthetic fluxes

Across the 43 sites in the US shown in Fig. 3, mean F_{s,O_3}^{syn} during the growing season ranges from 0.5 to 11.0 nmol O_3 m^{-2} s^{-1} with an average of 4.4 nmol O_3 m^{-2} s^{-1}. The highest F_{s,O_3}^{syn} generally occurs in the Midwest (5–9 nmol O_3 m^{-2} s^{-1} in Wisconsin, Michigan, Nebraska, and Ohio) due to its moderate O_3 concentrations (Fig. S6) and moisture levels, which promotes stomatal conductance (Fig. 1). The western US has higher average O_3 concentrations, but generally lower moisture and stomatal conductance, especially the southwestern US, so F_{s,O_3}^{syn} (0–4 nmol O_3 m^{-2} s^{-1}) is mostly lower than the Midwest. Land cover, land management, and plant types can drive large differences in F_{s,O_3}^{syn} between nearby sites, even when O_3 concentrations and meteorology are similar. For example, three Nebraska sites are all crop fields and O_3 concentrations are nearly identical, but two irrigated fields have higher stomatal conductance and higher F_{s,O_3}^{syn} than

the nearby rainfed field (6.2 vs. 4.8 nmol $O_3\,m^{-2}\,s^{-1}$). Two sites in central California have high g_s and F^{syn}_{s,O_3} compared to surrounding sites due to irrigation and naturally wet soil in the California Delta. A combination of topography and climate is also an important factor in California: forest sites in the Sierra Nevada have lower g_s and F^{syn}_{s,O_3} than the lowland crops and wetland grasses. In Oregon, an evergreen needleleaf site regrowing after a fire has higher g_s and F^{syn}_{s,O_3} than two older forest stands nearby. The differences between nine Wisconsin forest sites, however, are mostly due to different years of data at each site combined with interannual variability in F^{syn}_{s,O_3}; fluxes at these sites are similar in overlapping years.

Variability across the 60 sites in Europe is controlled by similar factors. Stomatal uptake ranges from 1.4 to 9.6 nmol $O_3\,m^{-2}\,s^{-1}$, with an average of 4.7 nmol $O_3\,m^{-2}\,s^{-1}$ (Fig. 3). The Mediterranean region has high O_3 concentrations (Fig. S8) but generally low stomatal conductance due to the dry climate (Fig. 1). Within this region, vegetation type explains broad patterns. Shrub sites in Spain, France, and Sardinia have very low g_s ($\sim 0.15\,cm\,s^{-1}$), so F^{syn}_{s,O_3} is low (1–3 nmol $O_3\,m^{-2}\,s^{-1}$), while most of the sites in mainland Italy are broadleaf and evergreen forests that have slightly greater g_s (~ 0.2–$0.4\,cm\,s^{-1}$) and F^{syn}_{s,O_3} (3–6 nmol $O_3\,m^{-2}\,s^{-1}$), despite similar climate and O_3. In central and northern Europe, temperate climate promotes higher stomatal conductance, while O_3 concentrations remain modest throughout the growing season. The largest F^{syn}_{s,O_3} is 9.8 nmol $O_3\,m^{-2}\,s^{-1}$ at a deciduous broadleaf forest in Switzerland, while nearby evergreen forests, cereal crops, and grasslands all have lower fluxes (6–8 nmol $O_3\,m^{-2}\,s^{-1}$). While Finland has a generally low F^{syn}_{s,O_3} of 2–5 nmol $O_3\,m^{-2}\,s^{-1}$, the high end of this range is similar to rural sites in Germany, illustrating that O_3 can impact remote ecosystems with high stomatal conductance, even where O_3 concentrations are low.

Table 2 quantifies SynFlux, O_3 deposition velocity, and conductance for each plant functional type. Wetlands, crops, and forests have the highest average F^{syn}_{s,O_3}, which is about 2 times higher than woody savanna or shrublands, the vegetation types with the lowest F^{syn}_{s,O_3}. At wetland sites, g_s and F^{syn}_{s,O_3} could be overestimated due to evaporation of surface water (Sect. 2.1), but any error is likely modest because our estimates of stomatal conductance at these sites ($0.48 \pm 0.16\,cm\,s^{-1}$; Table 2) are reasonable for wetland vegetation (up to $1\,cm\,s^{-1}$; Drake et al., 2013). The vegetation types rank in the same order for stomatal conductance, again showing stomata as the main control on O_3 uptake into vegetation. Stomatal uptake exceeds non-stomatal uptake for all plant functional types except woody savanna and shrubland. O_3 deposition velocities reported in Table 2 fall within the ranges of past literature, as reviewed by Silva and Heald (2017). However, while Silva and Heald found that the mean deposition velocity was greater over deciduous forests than coniferous forests, crops, or grass, we do not. Rather, we find that variability between sites within each of these categories is large, having a standard deviation of about 30 % of the multi-site mean.

4.2 Metrics for O_3 damage to plants

Since O_3 injures plants mainly by internal oxidative damage after entering the leaves through stomata, the most physiological predictor of plant injuries is the cumulative uptake of O_3 (CUO, Reich, 1987; Fuhrer, 2000; Karlsson et al., 2004; Cieslik, 2004; Matyssek et al., 2007). CUO is defined as the cumulative stomatal O_3 flux exceeding a threshold flux Y that can be detoxified by the plant, integrated over a period of time:

$$\mathrm{CUOY} = \sum_i H(F_{s,O_3,i} - Y)(F_{s,O_3,i} - Y)\,\Delta t_i.$$

Here, $H(x)$ is the Heaviside step function and Δt_i is the time elapsed during measurement of $F_{s,O_3,i}$. The sum is carried out over time i in the growing season, which we define based on GPP (Sect. 2.1). The detoxification threshold varies across vegetation types, even among related species (Karlsson et al., 2004; Büker et al., 2015), and thresholds for specific FLUXNET sites are generally unknown. As a compromise, we calculate CUO, with $Y = 0$, and also CUO3, with $Y = 3$ nmol $O_3\,m^{-2}\,s^{-1}$, which has been suggested as a reasonable generic threshold (Mills et al., 2011). CUO is always greater than CUO3, but the sites with high CUO tend to also have high CUO3, so their spatial patterns are similar (Fig. S8).

While CUO is a physiological dose, concentration-based metrics remain common for assessing ozone impacts because they are easier to measure. Concentration-based metrics quantify O_3 in ambient air irrespective of whether that O_3 enters leaves. These metrics follow the general form

$$M = \sum_i w(\chi_i)\,(\chi_i - \chi_c)\,\Delta t_i,$$

where $w(\chi)$ is a weighting function applied to the O_3 mole fraction χ, and χ_c is a constant. Like CUO, the sum is usually over time i during the growing season. Three of the most common concentration-based O_3 metrics are the mean O_3 concentration, the accumulated concentration over a threshold of 40 ppb (AOT40; UNECE, 2004), and the sigmoidal-weighted index (W126; Lefohn and Runeckles, 1987). For mean, $w(\chi) = \left(\sum \Delta t_i\right)^{-1}$ and $\chi_c = 0$. For AOT40, $w(\chi) = H(\chi - \chi_c)$ and $\chi_c = 40$ ppb. For W126, $w(\chi) = \left(1 + 4403\exp\left(-\left(126\,\mathrm{ppb}^{-1}\right)\chi\right)\right)^{-1}$ and $\chi_c = 0$. Both AOT40 and W126 use only daytime (08:00–20:00) measurements and W126 also takes the maximum value over all 3-month periods during the growing season. The weighting functions for AOT40 and W126 give little or no weight to O_3 concentrations below 40 ppb. In addition,

Table 2. Mean O_3 SynFlux, deposition velocity, and its conductance components during daytime in the growing season, grouped by plant functional type (PFT)[a].

PFT[b]	Sites	Site years	g_s	g_{ns}	g_c	v_d	$F_{O_3}^{syn}$	F_{s,O_3}^{syn}	CUO	CUO3
CRO	18	148	0.42 ± 0.17	0.28 ± 0.09	0.68 ± 0.18	0.53 ± 0.12	7.66 ± 1.96	4.77 ± 1.52	24.8 ± 12.4	14.9 ± 9.3
ENF	25	254	0.37 ± 0.10	0.25 ± 0.06	0.60 ± 0.11	0.54 ± 0.10	7.37 ± 1.33	4.61 ± 1.16	20.0 ± 5.69	11.9 ± 6.30
EBF	3	31	0.21 ± 0.02	0.15 ± 0.02	0.36 ± 0.03	0.33 ± 0.03	5.02 ± 0.65	2.90 ± 0.28	12.1 ± 0.81	5.12 ± 0.45
DBF	16	158	0.41 ± 0.14	0.20 ± 0.09	0.60 ± 0.18	0.53 ± 0.15	7.87 ± 2.28	5.37 ± 1.69	28.6 ± 13.8	15.7 ± 6.66
MF	5	83	0.44 ± 0.17	0.19 ± 0.01	0.62 ± 0.15	0.56 ± 0.14	7.82 ± 1.91	5.53 ± 2.15	24.9 ± 10.5	15.9 ± 8.90
WSA	2	25	0.10 ± 0.02	0.31 ± 0.06	0.39 ± 0.04	0.36 ± 0.04	6.14 ± 0.20	1.47 ± 0.31	6.46 ± 1.43	2.54 ± 1.72
OSH	4	14	0.19 ± 0.07	0.29 ± 0.10	0.47 ± 0.10	0.41 ± 0.09	5.69 ± 1.33	2.23 ± 0.87	8.60 ± 3.27	2.27 ± 1.54
CSH	2	15	0.27 ± 0.11	0.29 ± 0.01	0.57 ± 0.09	0.49 ± 0.05	6.78 ± 0.95	3.34 ± 1.24	14.3 ± 5.30	7.62 ± 5.49
GRA	18	136	0.40 ± 0.30	0.24 ± 0.11	0.64 ± 0.26	0.47 ± 0.15	7.04 ± 7.04	4.12 ± 2.45	18.3 ± 10.7	9.90 ± 6.98
WET[c]	10	53	0.48 ± 0.16	0.27 ± 0.09	0.74 ± 0.21	0.58 ± 0.14	8.80 ± 2.74	5.77 ± 2.08	25.1 ± 9.65	19.4 ± 15.6

[a] Values are the mean $\pm$ standard deviation across sites within each PFT. Units are cm s^{-1} for g_s, g_{ns}, g_c, and v_d; nmol O_3 m^{-2} s^{-1} for $F_{O_3}^{syn}$ and F_{s,O_3}^{syn}; and mmol O_3 m^{-2} for CUO and CUO3. [b] CRO: crop, ENF: evergreen needleleaf forest, EBF: evergreen broadleaf forest, DBF: deciduous broadleaf forest, MF: mixed forest, WSA: woody savanna, OSH: open shrubland, CSH: closed shrubland, GRA: grassland, WET: wetland. [c] Fluxes may be overestimated at wetland sites due to evaporation of surface water affecting the calculation of g_s, but any errors are likely modest because the g_s values here are reasonable (Drake et al., 2013).

W126 gives increasing weight to concentrations up to about 110 ppb and full weight for higher concentrations based on the understanding that exposure to high O_3 concentrations is more injurious than moderate or low concentrations. Other concentration-based metrics (e.g., SUM60) use other thresholds or weighting functions, but many are strongly correlated with AOT40 or W126 or otherwise qualitatively similar (Paoletti et al., 2007).

The spatial patterns of AOT40 and W126 closely resemble that of mean O_3 concentration in the US and Europe despite their different weighting functions (Fig. S9). AOT40 and W126 are well correlated with each other across sites ($R^2 = 0.87$) and with mean O_3 mole fraction ($R^2 = 0.76$ and $R^2 = 0.52$ for mean O_3 vs. AOT40 and W126, respectively) despite their different weighting functions. As a result, all of these concentration-based metrics have similar spatial patterns in the US and Europe. The CUO and CUO3 spatial patterns, however, are similar to F_{s,O_3}^{syn} and distinct from the concentration-based metrics. This illustrates that locations with high AOT40 or W126, like the southwestern US or Mediterranean Europe, can have low CUO.

Even though concentration-based metrics do not measure the physiological O_3 dose to plants, they can be useful if the metric is proportional to the flux-based dose and injuries. Indeed, many controlled experiments and observational studies have documented correlations between both AOT40 and W126 and either uptake or plant injuries (e.g., Fuhrer et al., 1997; Cieslik, 2004; Musselman et al., 2006; Matyssek et al., 2010). However, many of these studies were carried out at a single site or under conditions where stomatal conductance was relatively steady while O_3 concentrations varied, for example by maintaining well-watered soil. When stomatal conductance varies widely, such as between arid and humid climates or seasons, concentration-based metrics may not correlate with stomatal O_3 flux (Mills et al., 2011).

Figure 6 shows that all of the concentration-based metrics are poorly correlated with CUO across the sites (AOT40: $R^2 = 0.05$, W126: $R^2 = 0.03$, mean O_3: $R^2 = 0.04$). Humidity helps explain some of the scatter in Fig. 6. The sites with high concentration-based metrics and low CUO have high vapor pressure deficit (VPD) and low stomatal conductance, and are mostly in the western US and Mediterranean Europe. Restricting the analysis to humid sites (VPD < 1.5 kPa) does not improve the correlation ($R^2 \approx 0.05$) and at the arid sites (VPD > 1.6 kPa) the concentration-based metrics are modestly anti-correlated with CUO (AOT40: $R^2 = 0.19$, W126: $R^2 = 0.05$, mean O_3: $R^2 = 0.37$). This result reinforces that concentration-based metrics can misrepresent CUO and plant injuries (Mills et al., 2011).

From the CUO values in Table 2, we can estimate the range of O_3 impacts on biomass production at the FLUXNET sites. Although species vary in their sensitivity to O_3 (Lombardozzi et al., 2013), several studies suggest that the biomass production of broadleaf and needleleaf trees decreases by 0.2 % to 1 % per mmol O_3 m^{-2} of CUO (Karlsson et al., 2004; Wittig et al., 2007; Hoshika et al., 2015). Combining the mean CUO for each plant functional type (Table 2) with these sensitivities, our work implies that O_3 reduces the biomass production at these FLUXNET sites by 6 %–29 % for deciduous broadleaf forests and 4 %–20 % for needleleaf forests. The range represents the spread of reported dose–response sensitivities within each plant type, meaning the least and most O_3-sensitive species. Several broadleaf crops are more sensitive to O_3, with biomass reductions of 1.3 %–1.6 % per mmol O_3 m^{-2} of CUO3 (Mills et al., 2011). That sensitivity implies a 20 %–24 % drop in biomass production at FLUXNET crop sites. Some studies have quantified O_3 dose–response relationships with other thresholds $Y = 1.6$ to 6 nmol O_3 m^{-2} s^{-1} (e.g., Karlsson et al., 2007; Pleijel et al., 2004, 2014), but the sensitivities have a similar magnitude.

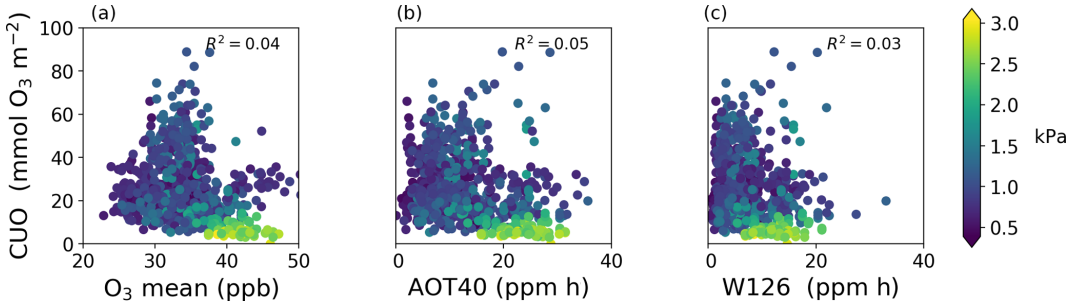

Figure 6. Comparison of cumulative uptake of O_3 (CUO) to concentration-based metrics of O_3 exposure during the daytime growing season at 103 sites: mean O_3 concentration **(a)**, AOT40 (center), and W126 **(b)**. There is one value (dot) per site per year. Colors show mean vapor pressure deficit during the growing season.

Fares et al. (2013) also demonstrated 12 %–19 % reduction in gross primary production due to O_3 at some of the same crop and forest FLUXNET sites. Using prognostic models of O_3 concentrations and stomatal uptake, several past studies have also suggested that O_3 reduces biomass production and CO_2 sequestration by 4 %–20 % in the US and Europe (Sitch et al., 2007; Wittig et al., 2007; Mills et al., 2011; Yue et al., 2014, 2016; Lombardozzi et al., 2015). Our results support this range of impacts, although some FLUXNET sites and species likely experience greater O_3 injury, but here the CUO is highly constrained from observations and therefore avoids the additional uncertainties of atmosphere–biosphere models.

5 Conclusions

We have demonstrated a method to estimate O_3 fluxes and stomatal O_3 uptake at eddy covariance flux towers wherever regional O_3 monitors exist. The method, called SynFlux, derives stomatal conductance and O_3 deposition velocity from standard eddy covariance measurements and combines them with gridded O_3 concentrations from air quality monitoring networks. We apply this method to the FLUXNET2015 dataset and derive synthetic flux estimates at 43 sites in the United States and 60 sites in Europe, totaling 926 site years of observations. O_3 deposition measurements have previously only been sporadically available for a few sites around the world, so this work dramatically increases the flux data available for understanding O_3 impacts on vegetation and for evaluating air quality and climate models.

Three sites with long-term O_3 flux measurements provide an independent test of SynFlux. These comparisons show that daily averages of synthetic stomatal F_{s,O_3}^{syn} correlate well with F_{s,O_3} observation-derived F_{s,O_3}^{obs} ($R^2 = 0.83$–0.93) and have a mean bias under 22 % at all sites. At all three sites 95 % of the synthetic F_{s,O_3}^{syn} values differ from measurements by a factor of 2 or less. The differences between F_{s,O_3}^{syn} and F_{s,O_3}^{obs} are also consistent with propagated uncertainty in the underlying measurements. Synthetic total deposition, $F_{O_3}^{syn}$, is sensitive to errors in the parameterized non-stomatal conductance, but mean values are still with a factor of 2 of observations. The errors in this dataset are modest compared with differences between observations and regional and global atmospheric chemistry models that are frequently a factor of 2 or more (Zhang et al., 2003; Hardacre et al., 2015; Clifton et al., 2017; Silva and Heald, 2017), illustrating the utility of this dataset for evaluating models and O_3 impacts.

Across flux tower sites in the US and Europe, F_{s,O_3}^{syn} ranges from 0.5 to 11.0 nmol O_3 m^{-2} s^{-1} during the summer growing season. The spatial pattern of F_{s,O_3}^{syn} is mainly controlled by stomatal conductance rather than O_3 concentration. Patterns of stomatal conductance and F_{s,O_3}^{syn} in turn are explained by climate, especially atmospheric and soil moisture, vegetation types, and land management, such as irrigation. O_3 concentration-based metrics (AOT40, W126, mean O_3) have been widely used to evaluate O_3 damages to plants because they are easier and cheaper to measure than the cumulative uptake of O_3 (CUO) into leaves. However, these metrics have very little correlation with CUO ($R^2 \leq 0.05$) across FLUXNET sites. Using dose–response relationships between CUO and biomass reduction, we estimate that O_3 reduces biomass production and carbon uptake by 4 %–29 %, depending on the site and plant type. Unlike most past estimates, which have used prognostic models of O_3 uptake, our assessment of biomass reduction is based on O_3 fluxes that are tightly constrained by observations. To promote further applications in ecosystem monitoring and modeling, the SynFlux dataset is publicly available as monthly averages of F_{s,O_3}^{syn}, $F_{O_3}^{syn}$, O_3 deposition velocity, stomatal conductance, and related variables.

Data availability. SynFlux data are archived and publicly available at https://doi.org/10.5281/zenodo.1402054 (Ducker et al., 2018).

The Supplement related to this article is available online at https://doi.org/10.5194/bg-15-5395-2018-supplement.

Competing interests. The authors declare that they have no conflict of interest.

Acknowledgements. This work was supported by the Winchester Fund and by the Council on Research Creativity at Florida State University. Eddy covariance data used here were acquired and shared by the FLUXNET community, including the AmeriFlux and CarboEuropeIP networks. The FLUXNET eddy covariance data processing and harmonization were carried out by the European Fluxes Database Cluster, AmeriFlux Management Project, and Fluxdata project of FLUXNET, with the support of CDIAC and the ICOS Ecosystem Thematic Center, and the OzFlux, ChinaFlux, and AsiaFlux offices. Trevor F. Keenan was supported by the Director, Office of Science, Office of Biological and Environmental Research of the US Department of Energy under contract DE-AC02-05CH11231 as part of the RUBISCO SFA. The O_3 concentration and flux measurements from Harvard Forest used in this analysis were supported by the National Science Foundation through the LTER program and various programs under the US Department of Energy Office of Science (BER). At Hyytiälä Forest, O_3 concentrations and flux measurements were supported by ICOS-Finland (281255) and the Academy of Finland Center of Excellence program (307331). At Blodgett Forest, O_3 concentrations and flux measurements were supported by ICOS-Finland (281255) and the Academy of Finland Center of Excellence program (307331). The long-term O_3 concentration and flux measurements from Blodgett Forest used in this analysis were supported by a combination of grants from the Kearney Foundation of Soil Science, the University of California Agricultural Experiment Station, the US Department of Energy Office of Science (BER), the National Science Foundation Atmospheric Chemistry Program, and the California Air Resources Board.

Edited by: Lutz Merbold
Reviewed by: two anonymous referees

References

Acosta, M., Pavelka, M., Montagnani, L., Kutsch, W., Lindroth, A., Juszczak, R., and Janouš, D.: Soil surface CO2 efflux measurements in Norway spruce forests: Comparison between four different sites across Europe – from boreal to alpine forest, Geoderma, 192, 295–303, https://doi.org/10.1016/j.geoderma.2012.08.027, 2013.

Ainsworth, E. A. and Long, S. P.: What have we learned from 15 years of free-air CO_2 enrichment (FACE)? A meta-analytic review of the responses of photosynthesis, canopy properties and plant production to rising CO_2, New Phytol., 165, 351–372, https://doi.org/10.1111/j.1469-8137.2004.01224.x, 2005.

Ainsworth, E. E. A., Yendrek, C. R., Sitch, S., Collins, W. J., and Emberson, L. D.: The effects of tropospheric ozone on net primary productivity and implications for climate change, Annu. Rev. Plant Biol., 63, 637–61, https://doi.org/10.1146/annurev-arplant-042110-103829, 2012.

Altimir, N., Kolari, P., Tuovinen, J., Vesala, T., Bäck, J., Suni, T., Hari, P., Altimir, N., Kolari, P., Tuovinen, J., Vesala, T., and Bäck, J.: Foliage surface ozone deposition: a role for surface moisture?, Biogeosciences, 3, 209–228, https://doi.org/10.5194/bg-3-209-2006.

Ammann, C., Spirig, C., Leifeld, J., and Neftel, A.: Assessment of the nitrogen and carbon budget of two managed temperate grassland fields, Agr. Ecosyst. Environ., 133, 150–162, https://doi.org/10.1016/j.agee.2009.05.006, 2009.

Anderson, D. E., Verma, S. B., and Rosenberg, N. J.: Eddy correlation measurements of CO_2, latent heat, and sensible heat fluxes over a crop surface, Bound.-Lay. Meteorol., 29, 263–272, https://doi.org/10.1007/BF00119792, 1984.

Anthoni, P. M., Knohl, A., Rebmann, C., Freibauer, A., Mund, M., Ziegler, W., Kolle, O., and Schulze, E.-D.: Forest and agricultural land-use-dependent CO_2 exchange in Thuringia, Germany, Glob. Change Biol., 10, 2005–2019, https://doi.org/10.1111/j.1365-2486.2004.00863.x, 2004.

Aubinet, M., Chermanne, B., Vandenhaute, M., Longdoz, B., Yernaux, M., and Laitat, E.: Long term carbon dioxide exchange above a mixed forest in the Belgian Ardennes, Agr. Forest Meteorol., 108, 293–315, https://doi.org/10.1016/s0168-1923(01)00244-1, 2001.

Avnery, S., Mauzerall, D. L., Liu, J., and Horowitz, L. W.: Global crop yield reductions due to surface ozone exposure: 1. Year 2000 crop production losses and economic damage, Atmos. Environ., 45, 2284–2296, https://doi.org/10.1016/j.atmosenv.2010.11.045, 2011.

Baldocchi, D.: AmeriFlux US-Tw4 Twitchell East End Wetland, Ameriflux, Univ. of Califronia, Berkeley, CA, USA, https://doi.org/10.17190/AMF/1246151, 2016.

Baldocchi, D., Falge, E., Gu, L., Olson, R., Hollinger, D., Running, S., Anthoni, P., Bernhofer, C., Davis, K., Evans, R., Fuentes, J., Goldstein, A., Katul, G., Law, B., Lee, X., Malhi, Y., Meyers, T., Munger, W., Oechel, W., Paw, U. K. T., Pilegaard, K., Schmid, H. P., Valentini, R., Verma, S., Vesala, T., Wilson, K., and Wofsy, S.: FLUXNET: A new tool to study the temporal and spatial variability of ecosystem-scale carbon dioxide, water vapor, and energy flux densities, B. Am. Meteorol. Soc., 82, 2415–2434, https://doi.org/10.1175/1520-0477(2001)082<2415:FANTTS>2.3.CO;2, 2001.

Baldocchi, D., Chen, Q., Chen, X., Ma, S., Miller, G., Ryu, Y., Xiao, J., Wenk, R., and Battles, J.: The dynamics of energy, water, and carbon fluxes in a blue oak (Quercus douglasii) savanna in California, Ecosyst. Funct. Savannas, 1, 135–151, https://doi.org/10.1201/b10275-10, 2010.

Berbigier, P., Bonnefond, J.-M., and Mellmann, P.: CO_2 and water vapour fluxes for 2 years above Euroflux forest site, Agr. Forest Meteorol., 108, 183–197, https://doi.org/10.1016/s0168-1923(01)00240-4, 2001.

Bonan, G. B., Lawrence, P. J., Oleson, K. W., Levis, S., Jung, M., Reichstein, M., Lawrence, D. M., and Swenson, S. C.: Improving canopy processes in the Community Land Model version 4 (CLM4) using global flux fields empirically inferred from FLUXNET data, J. Geophys. Res., 116, G02014, https://doi.org/10.1029/2010JG001593, 2011.

Bowling, D. R., Bethers-Marchetti, S., Lunch, C. K., Grote, E. E., and Belnap, J.: Carbon, water, and energy fluxes in a semiarid cold desert grassland during and following multiyear drought, J. Geophys. Res., 115, G04026, https://doi.org/10.1029/2010jg001322, 2010.

Büker, P., Feng, Z., Uddling, J., Briolat, A., Alonso, R., Braun, S., Elvira, S., Gerosa, G., Karlsson, P. E., Le Thiec, D., Marzuoli, R., Mills, G., Oksanen, E., Wieser, G., Wilkinson, M., and Emberson, L. D.: New flux based dose-response relationships for ozone for European forest tree species, Environ. Pollut., 206, 163–174, https://doi.org/10.1016/j.envpol.2015.06.033, 2015.

Carrara, A., Janssens, I. A., Yuste, J. C., and Ceulemans, R.: Seasonal changes in photosynthesis, respiration and NEE of a mixed temperate forest, Agr. Forest Meteorol., 126, 15–31, https://doi.org/10.1016/j.agrformet.2004.05.002, 2004.

Chiesi, M., Maselli, F., Bindi, M., Fibbi, L., Cherubini, P., Arlotta, E., Tirone, G., Matteucci, G., and Seufert, G.: Modelling carbon budget of Mediterranean forests using ground and remote sensing measurements, Agr. Forest Meteorol., 135, 22–34, https://doi.org/10.1016/j.agrformet.2005.09.011, 2005.

Cieslik, S. A.: Ozone uptake by various surface types: A comparison between dose and exposure, Atmos. Environ., 38, 2409–2420, https://doi.org/10.1016/j.atmosenv.2003.10.063, 2004.

Claverie, M., Vermote, E. F., Weiss, M., Baret, F., Hagolle, O., and Demarez, V.: Validation of coarse spatial resolution LAI and FAPAR time series over cropland in southwest France, Remote Sens. Environ., 139, 216–230, https://doi.org/10.1016/j.rse.2013.07.027, 2013.

Claverie, M., Matthews, J. L., Vermote, E. F., and Justice, C. O.: A 30 + Year AVHRR LAI and FAPAR Climate Data Record?: Algorithm Description and Validation, Remote Sens., 8, 1–12, https://doi.org/10.3390/rs8030263, 2016.

Clifton, O. E., Fiore, A. M., Munger, J. W., Malyshev, S., Horowitz, L. W., Shevliakova, E., Paulot, F., Murray, L. T., and Griffin, K. L.: Interannual variability in ozone removal by a temperate deciduous forest, Geophys. Res. Lett., 44, 542–552, https://doi.org/10.1002/2016GL070923, 2017.

Cook, B. D., Davis, K. J., Wang, W., Desai, A., Berger, B. W., Teclaw, R. M., Martin, J. G., Bolstad, P. V., Bakwin, P. S., Yi, C., and Heilman, W.: Carbon exchange and venting anomalies in an upland deciduous forest in northern Wisconsin, USA, Agr. Forest Meteorol., 126, 271–295, https://doi.org/10.1016/j.agrformet.2004.06.008, 2004.

Delpierre, N., Berveiller, D., Granda, E., and Dufrêne, E.: Wood phenology, not carbon input, controls the interannual variability of wood growth in a temperate oak forest, New Phytol., 210, 459–470, https://doi.org/10.1111/nph.13771, 2015.

Desai, A. R., Bolstad, P. V., Cook, B. D., Davis, K. J., and Carey, E. V.: Comparing net ecosystem exchange of carbon dioxide between an old-growth and mature forest in the upper Midwest, USA, Agr. Forest Meteorol., 128, 33–55, https://doi.org/10.1016/j.agrformet.2004.09.005, 2005.

Desai, A. R., Xu, K., Tian, H., Weishampel, P., Thom, J., Baumann, D., Andrews, A. E., Cook, B. D., King, J. Y., and Kolka, R.: Landscape-level terrestrial methane flux observed from a very tall tower, Agr. Forest Meteorol., 201, 61–75, https://doi.org/10.1016/j.agrformet.2014.10.017, 2015.

Dietiker, D., Buchmann, N., and Eugster, W.: Testing the ability of the DNDC model to predict CO_2 and water vapour fluxes of a Swiss cropland site, Agr. Ecosyst. Environ., 139, 396–401, https://doi.org/10.1016/j.agee.2010.09.002, 2010.

Dolman, A. J., Moors, E. J., and Elbers, J. A.: The carbon uptake of a mid latitude pine forest growing on sandy soil, Agr. Forest Meteorol., 111, 157–170, https://doi.org/10.1016/S0168-1923(02)00024-2, 2002.

Dragoni, D., Schmid, H. P., Wayson, C. A., Potter, H., Grimmond, C. S. B., and Randolph, J. C.: Evidence of increased net ecosystem productivity associated with a longer vegetated season in a deciduous forest in south-central Indiana, USA, Glob. Change Biol., 17, 886–897, https://doi.org/10.1111/j.1365-2486.2010.02281.x, 2011.

Drake, P. L., Froend, R. H., and Franks, P. J.: Smaller, faster stomata?: scaling of stomatal size, rate of response, and stomatal conductance, Exp. Bot., 64, 495–505, https://doi.org/10.1093/jxb/ers347, 2013.

Ducker, J. A., Holmes, C. D., Keenan, T. F., Fares, S., Goldstein, A. H., Mammarella, I., Munger, J. W., and Schnell, J.: Synthetic ozone depsoition and stomatal uptake at flux tower sites, Biogeosciences Discuss., https://doi.org/10.5194/bg-2018-172, 2018.

Dušek, J., Čížková, H., Stellner, S., Czerný, R., and Květ, J.: Fluctuating water table affects gross ecosystem production and gross radiation use efficiency in a sedge-grass marsh, Hydrobiologia, 692, 57–66, https://doi.org/10.1007/s10750-012-0998-z, 2012.

El-Madany, T., Niklasch, K., and Klemm, O.: Stomatal and non-stomatal turbulent deposition flux of ozone to a managed peatland, Atmosphere, 8, p. 175, https://doi.org/10.3390/atmos8090175, 2017.

Etzold, S., Ruehr, N. K., Zweifel, R., Dobbertin, M., Zingg, A., Pluess, P., Häsler, R., Eugster, W., and Buchmann, N.: The carbon balance of two contrasting mountain forest ecosystems in Switzerland: Similar annual trends, but seasonal differences, Ecosystems, 14, 1289–1309, https://doi.org/10.1007/s10021-011-9481-3, 2011.

Fares, S., McKay, M., Holzinger, R., and Goldstein, A. H.: Ozone fluxes in a Pinus ponderosa ecosystem are dominated by non-stomatal processes: Evidence from long-term continuous measurements, Agr. Forest Meteorol., 150, 420–431, https://doi.org/10.1016/j.agrformet.2010.01.007, 2010.

Fares, S., Vargas, R., Detto, M., Goldstein, A. H., Karlik, J., Paoletti, E., and Vitale, M.: Tropospheric ozone reduces carbon assimilation in trees: Estimates from analysis of continuous flux measurements, Glob. Change Biol., 19, 2427–2443, doi:10.1111/gcb.12222, 2013.

Fares, S., Savi, F., Muller, J., Matteucci, G., and Paoletti, E.: Simultaneous measurements of above and below canopy ozone fluxes help partitioning ozone deposition between its various sinks in a Mediterranean Oak Forest, Agr. Forest Meteorol., 198/199, 181–191, https://doi.org/10.1016/j.agrformet.2014.08.014, 2014.

Ferréa, C., Zenone, T., Comolli, R., and Seufert, G.: Estimating heterotrophic and autotrophic soil respiration in a semi-natural forest of Lombardy, Italy, Pedobiologia, 55, 285–294, https://doi.org/10.1016/j.pedobi.2012.05.001, 2012.

Finkelstein, P. L., Ellestad, T. G., Clarke, J. F., Meyers, T. P., Schwede, D. B., Hebert, E. O., and Neal, J. A.: Ozone and sulfur dioxide dry deposition to forests: Observations and model evaluation, J. Geophys. Res.-Atmos., 105, 15365–15377, https://doi.org/10.1029/2000JD900185, 2000.

Fischer, M. L., Billesbach, D. P., Berry, J. A., Riley, W. J., and Torn, M. S.: Spatiotemporal variations in growing season exchanges of CO_2, H_2O, and sensible heat in agricultural fields of the Southern Great Plains, Earth Interact., 11, 1–21, https://doi.org/10.1175/ei231.1, 2007.

Fowler, D., Flechard, C., Cape, J. N., Storeton-West, R. L., and Coyle M.: Measurements of ozone deposition to vegetation quantifying the flux, the stomatal and non-stomatal components, Water. Air. Soil Pollut., 130, 63–74, https://doi.org/10.1023/A:1012243317471, 2001.

Foken, T.: Micrometeorology, 2nd Edn., Springer, 2, 1–326, https://doi.org/10.1007/978-3-642-25440-6, 2017.

Frank, J. M., Massman, W. J., Ewers, B. E., Huckaby, L. S., and Negrón, J. F.: Ecosystem CO_2 / H_2O fluxes are explained by hydraulically limited gas exchange during tree mortality from spruce bark beetles, J. Geophys. Res.-Biogeo., 119, 1195–1215, https://doi.org/10.1002/2013jg002597, 2014.

Fuhrer, J.: Introduction to the special issue on ozone risk analysis for vegetation in Europe, Environ. Pollut., 109, 359–360, 2000.

Fuhrer, J., Skärby, L., and Ashmore, M. R.: Critical levels for ozone effects on vegetation in Europe, Environ. Pollut., 97, 91–106, https://doi.org/10.1016/S0269-7491(97)00067-5, 1997.

Galvagno, M., Wohlfahrt, G., Cremonese, E., Rossini, M., Colombo, R., Filippa, G., Julitta, T., Manca, G., Siniscalco, C., di Cella, U. M., and Migliavacca, M.: Phenology and carbon dioxide source/sink strength of a subalpine grassland in response to an exceptionally short snow season, Environ. Res. Lett., 8, 25008, https://doi.org/10.1088/1748-9326/8/2/025008, 2013.

Garbulsky, M. F., Penuelas, J., Papale, D., and Filella, I.: Remote estimation of carbon dioxide uptake by a Mediterranean forest, Glob. Change Biol., 14, 2860–2867, https://doi.org/10.1111/j.1365-2486.2008.01684.x, 2008.

Gelaro, R., McCarty, W., Suárez, M. J., Todling, R., Molod, A., Takacs, L., Randles, C. A., Darmenov, A., Bosilovich, M. G., Reichle, R., Wargan, K., Coy, L., Cullather, R., Draper, C., Akella, S., Buchard, V., Conaty, A., da Silva, A. M., Gu, W., Kim, G. K., Koster, R., Lucchesi, R., Merkova, D., Nielsen, J. E., Partyka, G., Pawson, S., Putman, W., Rienecker, M., Schubert, S. D., Sienkiewicz, M., and Zhao, B.: The modern-era retrospective analysis for research and applications, version 2 (MERRA-2), J. Clim., 30, 5419–5454, https://doi.org/10.1175/JCLI-D-16-0758.1, 2017.

Gentine, P., Chhang, A., Rigden, A., and Salvucci, G.: Evaporation estimates using weather station data and boundary layer theory, Geophys. Res. Lett., 43, 661–670, https://doi.org/10.1002/2016GL070819, 2016.

Gerosa, G., Marzuoli, R., Cieslik, S., and Ballarin-Denti, A.: Stomatal ozone fluxes over a barley field in Italy, "Effective exposure" as a possible link between exposure- and flux-based approaches, Atmos. Environ., 38, 2421–2432, https://doi.org/10.1016/j.atmosenv.2003.12.040, 2004.

Gerosa, G., Vitale, M., Finco, A., Manes, F., Denti, A. B., and Cieslik, S.: Ozone uptake by an evergreen Mediterranean Forest (Quercus ilex) in Italy. Part I: Micrometeorological flux measurements and flux partitioning, Atmos. Environ., 39, 3255–3266, https://doi.org/10.1016/j.atmosenv.2005.01.056, 2005.

Gerosa, G., Derghi, F., and Cieslik, S.: Comparison of different algorithms for stomatal ozone flux determination from micrometeorological measurements, Water. Air. Soil Pollut., 179, 309–321, https://doi.org/10.1007/s11270-006-9234-7, 2007.

Goldstein, A. H., Hultman, N. E., Fracheboud, J. M., Bauer, M. R., Panek, J. A., Xu, M., Qi, Y., Guenther, A. B., and Baugh, W.: Effects of climate variability on the carbon dioxide, water, and sensible heat fluxes above a ponderosa pine plantation in the Sierra Nevada (CA), Agr. Forest Meteorol., 101, 113–129, https://doi.org/10.1016/S0168-1923(99)00168-9, 2000.

Gough, C. M., Hardiman, B. S., Nave, L. E., Bohrer, G., Maurer, K. D., Vogel, C. S., Nadelhoffer, K. J., and Curtis, P. S.: Sustained carbon uptake and storage following moderate disturbance in a Great Lakes forest, Ecol. Appl., 23, 1202–1215, https://doi.org/10.1890/12-1554.1, 2013.

Grünwald, T. and Bernhofer, C.: A decade of carbon, water and energy flux measurements of an old spruce forest at the Anchor Station Tharandt, Tellus B, 59, 387–396, https://doi.org/10.3402/tellusb.v59i3.17000, 2007.

Guidi, L., Nali, C., Lorenzini, G., Filippi, F., and Soldatini, G. F.: Effect of chronic ozone fumigation on the photosynthetic process of poplar clones showing different sensitivity, Environ. Pollut., 113, 245–254, https://doi.org/10.1016/S0269-7491(00)00194-9, 2001.

Hardacre, C., Wild, O., and Emberson, L.: An evaluation of ozone dry deposition in global scale chemistry climate models, Atmos. Chem. Phys., 15, 6419–6436, https://doi.org/10.5194/acp-15-6419-2015, 2015.

Hatala, J. A., Detto, M., Sonnentag, O., Deverel, S. J., Verfaillie, J., and Baldocchi, D. D.: Greenhouse gas (CO_2, CH_4, H_2O) fluxes from drained and flooded agricultural peatlands in the Sacramento-San Joaquin Delta, Agr. Ecosyst. Environ., 150, 1–18, https://doi.org/10.1016/j.agee.2012.01.009, 2012.

Holtslag, A. A. M. and De Bruin, H. A. R.: Applied modeling of the nighttime surface energy balance over land, J. Appl. Meteorol., 27, 689–704, https://doi.org/10.1175/1520-0450(1988)027<0689:AMOTNS>2.0.CO;2, 1988.

Hommeltenberg, J., Schmid, H. P., Drösler, M., and Werle, P.: Can a bog drained for forestry be a stronger carbon sink than a natural bog forest?, Biogeosciences, 11, 3477–3493, https://doi.org/10.5194/bg-11-3477-2014, 2014.

Hoshika, Y., Katata, G., Deushi, M., Watanabe, M., Koike, T., and Paoletti, E.: Ozone-induced stomatal sluggishness changes carbon and water balance of temperate deciduous forests, Sci. Rep., 5, 9871, https://doi.org/10.1038/srep09871, 2015.

Imer, D., Merbold, L., Eugster, W., and Buchmann, N.: Temporal and spatial variations of soil CO_2, CH_4 and N_2O fluxes at three differently managed grasslands, Biogeosciences, 10, 5931–5945, https://doi.org/10.5194/bg-10-5931-2013, 2013.

Irvine, J., Law, B. E., and Hibbard, K. A.: Postfire carbon pools and fluxes in semiarid ponderosa pine in Central Oregon, Glob. Change Biol., 13, 1748–1760, https://doi.org/10.1111/j.1365-2486.2007.01368.x, 2007.

Irvine, J., Law, B. E., Martin, J. G., and Vickers, D.: Interannual variation in soil CO_2 efflux and the response of root respiration to climate and canopy gas exchange in mature ponderosa pine, Glob. Change Biol., 14, 2848–2859, https://doi.org/10.1111/j.1365-2486.2008.01682.x, 2008.

Jacobs, C. M. J., Jacobs, A. F. G., Bosveld, F. C., Hendriks, D. M. D., Hensen, A., Kroon, P. S., Moors, E. J., Nol, L., Schrier-Uijl, A., and Veenendaal, E. M.: Variability of annual CO2 exchange from Dutch grasslands, Biogeosciences, 4, 803–816, https://doi.org/10.5194/bg-4-803-2007, 2007.

Jacobson, M. Z.: Fundamentals of atmospheric modeling second edition, Cambridge University Press, 1–707, 2005.

Karlsson, P. E., Uddling, J., Braun, S., Broadmeadow, M., Elvira, S., Gimeno, B. S., Le Thiec, D., Oksanen, E., Vandermeiren,

K., Wilkinson, M., and Emberson, L.: New critical levels for ozone effects on young trees based on AOT40 and simulated cumulative leaf uptake of ozone, Atmos. Environ., 38, 2283–2294, https://doi.org/10.1016/j.atmosenv.2004.01.027, 2004.

Kavassalis, S. C. and Murphy, J. G.: Understanding ozone-meteorology correlations: A role for dry deposition, Geophys. Res. Lett., 44, 2922–2931, https://doi.org/10.1002/2016GL071791, 2017.

Keronen, P., Reissell, A., Rannik, Ü., Pohja, T., Siivola, E., Hiltunen, V., Hari, P., Kulmala, M., and Vesala, T.: Ozone flux measurements over a Scots pine forest using eddy covariance method: Performance evaluation and comparison with flux-profile method, Boreal Environ. Res., 8, 425–443, 2003.

Knauer, J., Zaehle, S., Medlyn, B. E., Reichstein, M., Werner, C., Keitel, C., Williams, C. A., Migliavacca, M., Kauwe, M. G. De, Kolari, P., Limousin, J.-M., and Linderson, M.-L.: Towards physiologically meaningful water-use efficiency estimates from eddy covariance data, Glob. Change Biol., 15, 694–710, https://doi.org/10.1111/gcb.13893, 2017.

Knohl, A., Schulze, E.-D., Kolle, O., and Buchmann, N.: Large carbon uptake by an unmanaged 250-year-old deciduous forest in Central Germany, Agr. Forest Meteorol., 118, 151–167, https://doi.org/10.1016/s0168-1923(03)00115-1, 2003.

Knox, S. H., Matthes, J. H., Sturtevant, C., Oikawa, P. Y., Verfaillie, J., and Baldocchi, D.: Biophysical controls on interannual variability in ecosystem-scale CO_2 and CH_4 exchange in a California rice paddy, J. Geophys. Res.-Biogeo., 121, 978–1001, https://doi.org/10.1002/2015jg003247, 2016.

Kurbatova, J., Li, C., Varlagin, A., Xiao, X., and Vygodskaya, N.: Modeling carbon dynamics in two adjacent spruce forests with different soil conditions in Russia, Biogeosciences, 5, 969–980, https://doi.org/10.5194/bg-5-969-2008, 2008.

Kurpius, M. R. and Goldstein, A. H.: Gas-phase chemistry dominates O_3 loss to a forest, implying a source of aerosols and hydroxyl radicals to the atmosphere, Geophys. Res. Lett., 30, 2–5, https://doi.org/10.1029/2002GL016785, 2003.

Lamaud, E., Loubet, B., Irvine, M., Stella, P., Personne, E., and Cellier, P.: Partitioning of ozone deposition over a developed maize crop between stomatal and non-stomatal uptakes, using eddy-covariance flux measurements and modelling, Agr. Forest Meteorol., 149, 1385–1396, https://doi.org/10.1016/j.agrformet.2009.03.017, 2009.

Launiainen, S., Rinne, J., Pumpanen, J., Kulmala, L., Kolari, P., Keronen, P., Siivola, E., Pohja, T., Hari, P., and Vesala, T.: Eddy covariance measurements of CO_2 and sensible and latent heat fluxes during a full year in a boreal pine forest trunk-space, Boreal Environ. Res., 10, 569–588, 2005.

Lefohn, A. S. and Runeckles, V. C.: Establishing standards to protect vegetation-ozone exposure/dose considerations, Atmos. Environ., 21, 561–568, https://doi.org/10.1016/0004-6981(87)90038-2, 1987.

Lin, C., Gentine, P., Huang, Y., Guan, K., Kimm, H., and Zhou, S.: Diel ecosystem conductance response to vapor pressure deficit is suboptimal and independent of soil moisture, Agr. Forest Meteorol., 250/251, 24–34, https://doi.org/10.1016/j.agrformet.2017.12.078, 2018.

Lindauer, M., Schmid, H. P., Grote, R., Mauder, M., Steinbrecher, R., and Wolpert, B.: Net ecosystem exchange over a non-cleared wind-throw-disturbed upland spruce forest – Measurements and simulations, Agr. Forest Meteorol., 197, 219–234, https://doi.org/10.1016/j.agrformet.2014.07.005, 2014.

Lohila, A.: Annual CO_2 exchange of a peat field growing spring barley or perennial forage grass, J. Geophys. Res., 109, D18116, https://doi.org/10.1029/2004jd004715, 2004.

Lombardozzi, D., Sparks, J. P., Bonan, G., and Levis, S.: Ozone exposure causes a decoupling of conductance and photosynthesis: Implications for the Ball-Berry stomatal conductance model, Oecologia, 169, 651–659, https://doi.org/10.1007/s00442-011-2242-3, 2012.

Lombardozzi, D., Sparks, J. P., and Bonan, G.: Integrating O_3 influences on terrestrial processes: photosynthetic and stomatal response data available for regional and global modeling, Biogeosciences, 10, 6815–6831, https://doi.org/10.5194/bg-10-6815-2013, 2013.

Lombardozzi, D., Levis, S., Bonan, G., Hess, P. G., and Sparks, J. P.: The influence of chronic ozone exposure on global carbon and water cycles, J. Clim., 28, 292–305, https://doi.org/10.1175/JCLI-D-14-00223.1, 2015.

Loubet, B., Laville, P., Lehuger, S., Larmanou, E., Fléchard, C., Mascher, N., Genermont, S., Roche, R., Ferrara, R. M., Stella, P., Personne, E., Durand, B., Decuq, C., Flura, D., Masson, S., Fanucci, O., Rampon, J.-N., Siemens, J., Kindler, R., Gabrielle, B., Schrumpf, M., and Cellier, P.: Carbon, nitrogen and Greenhouse gases budgets over a four years crop rotation in northern France, Plant Soil, 343, 109–137, https://doi.org/10.1007/s11104-011-0751-9, 2011.

Ma, S., Baldocchi, D. D., Xu, L., and Hehn, T.: Inter-annual variability in carbon dioxide exchange of an oak/grass savanna and open grassland in California, Agr. Forest Meteorol., 147, 157–171, https://doi.org/10.1016/j.agrformet.2007.07.008, 2007.

Mammarella, I., Kolari, P., Rinne, J., Keronen, P., Pumpanen, J., and Vesala, T.: Determining the contribution of vertical advection to the net ecosystem exchange at Hyytiälä forest, Finland, Tellus B, 59, 900–909, https://doi.org/10.1111/j.1600-0889.2007.00306.x, 2007.

Marcolla, B., Pitacco, A., and Cescatti, A.: Canopy architecture and turbulence structure in a coniferous forest, Bound.-Lay. Meteorol., 108, 39–59, https://doi.org/10.1023/a:1023027709805, 2003.

Marcolla, B., Cescatti, A., Manca, G., Zorer, R., Cavagna, M., Fiora, A., Gianelle, D., Rodeghiero, M., Sottocornola, M., and Zampedri, R.: Climatic controls and ecosystem responses drive the inter-annual variability of the net ecosystem exchange of an alpine meadow, Agr. Forest Meteorol., 151, 1233–1243, https://doi.org/10.1016/j.agrformet.2011.04.015, 2011.

Marrero, T. R. and Mason, E. A.: Gaseous Diffusion Coefficients, J. Phys. Chem. Ref. Data, 1, 3–118, https://doi.org/10.1063/1.3253094, 1972.

Matthes, J. H., Sturtevant, C., Verfaillie, J., Knox, S., and Baldocchi, D.: Parsing the variability in CH_4 flux at a spatially heterogeneous wetland: Integrating multiple eddy covariance towers with high-resolution flux footprint analysis, J. Geophys. Res.-Biogeo., 119, 1322–1339, https://doi.org/10.1002/2014jg002642, 2014.

Matyssek, R., Bahnweg, G., Ceulemans, R., Fabian, P., Grill, D., Hanke, D. E., Kraigher, H., Oßwald, W., Rennenberg, H., Sandermann, H., Tausz, M., and Wieser, G.: Synopsis of the CASIROZ case study: Carbon sink strength of *Fagus sylvatica* L. in a changing environment – Experimental risk assessment

of mitigation by chronic ozone impact, Plant Biol., 9, 163–180, https://doi.org/10.1055/s-2007-964883, 2007.

Matyssek, R., Karnosky, D. F., Wieser, G., Percy, K., Oksanen, E., Grams, T. E. E., Kubiske, M., Hanke, D., and Pretzsch, H.: Advances in understanding ozone impact on forest trees: Messages from novel phytotron and free-air fumigation studies, Environ. Pollut., 158, 1990–2006, https://doi.org/10.1016/j.envpol.2009.11.033, 2010.

Mauder, M., Cuntz, M., Drüe, C., Graf, A., Rebmann, C., Schmid, H. P., Schmidt, M., and Steinbrecher, R.: A strategy for quality and uncertainty assessment of long-term eddy-covariance measurements, Agr. Forest Meteorol., 169, 122–135, https://doi.org/10.1016/j.agrformet.2012.09.006, 2013.

McKinney, W.: Data Structures for Statistical Computing in Python, in: Proceedings of the 9th Python in Science Conference, edited by: Van Der Walt, S., 51–56., 2010.

Medlyn, B. E., Duursma, R. A., Eamus, D., Ellsworth, D. S., Prentice, I. C., Barton, C. V. M., Crous, K. Y., De Angelis, P., Freeman, M., and Wingate, L.: Reconciling the optimal and empirical approaches to modelling stomatal conductance, Glob. Change Biol., 17, 2134–2144, https://doi.org/10.1111/j.1365-2486.2010.02375.x, 2011.

Merbold, L., Eugster, W., Stieger, J., Zahniser, M., Nelson, D., and Buchmann, N.: Greenhouse gas budget (CO_2, CH_4, and N_2O) of intensively managed grassland following restoration, Glob. Change Biol., 20, 1913–1928, https://doi.org/10.1111/gcb.12518, 2014.

Migliavacca, M., Meroni, M., Busetto, L., Colombo, R., Zenone, T., Matteucci, G., Manca, G., and Seufert, G.: Modeling gross primary production of agro-forestry ecosystems by assimilation of satellite-derived information in a process-based model, Sensors, 9, 922–942, https://doi.org/10.3390/s90200922, 2009.

Mills, G., Hayes, F., Simpson, D., Emberson, L., Norris, D., Harmens, H., and Büker, P.: Evidence of widespread effects of ozone on crops and (semi-)natural vegetation in Europe (1990–2006) in relation to AOT40- and flux-based risk maps, Glob. Change Biol., 17, 592–613, https://doi.org/10.1111/j.1365-2486.2010.02217.x, 2011.

Monson, R. K., Turnipseed, A. A., Sparks, J. P., Harley, P. C., Scott-Denton, L. E., Sparks, K., and Huxman, T. E.: Carbon sequestration in a high-elevation, subalpine forest, Glob. Change Biol., 8, 459–478, https://doi.org/10.1046/j.1365-2486.2002.00480.x, 2002.

Montagnani, L., Manca, G., Canepa, E., Georgieva, E., Acosta, M., Feigenwinter, C., Janous, D., Kerschbaumer, G., Lindroth, A., Minach, L., Minerbi, S., Mölder, M., Pavelka, M., Seufert, G., Zeri, M., and Ziegler, W.: A new mass conservation approach to the study of CO_2 advection in an alpine forest, J. Geophys. Res., 114, D07306, https://doi.org/10.1029/2008jd010650, 2009.

Monteith, J. L.: Evaporation and surface temperature, Q. J. Roy. Meteor. Soc., 107, 1–27, 1981.

Moore, K. E., Fitzjarrald, D. R., Sakai, R. K., Goulden, M. L., Munger, J. W., and Wofsy, S. C.: Seasonal variation in radiative and turbulent exchange at a deciduous forest in central Massachusetts, J. Appl. Meterol., 35, 122–134, https://doi.org/10.1175/1520-0450(1996)035<0122:SVIRAT>2.0.CO;2, 1996.

Morin, T. H., Bohrer, G. D. M., Frasson, R. P., Naor-Azreli, L., Mesi, S., Stefanik, K. C., and Schäfer, K. V. R.: Environmental drivers of methane fluxes from an urban temperate wetland park, J. Geophys. Res.-Biogeo., 119, 2188–2208, https://doi.org/10.1002/2014jg002750, 2014.

Moureaux, C., Debacq, A., Bodson, B., Heinesch, B., and Aubinet, M.: Annual net ecosystem carbon exchange by a sugar beet crop, Agr. Forest Meteorol., 139, 25–39, https://doi.org/10.1016/j.agrformet.2006.05.009, 2006.

Munger, J. W., Wofsy, S. C., Bakwin, P. S., Fan, S., Goulden, M. L., Daube, B. C., Goldstein, A. H., Moore, K. E., and Fitzjarrald, D. R.: Atmospheric deposition of reactive nitrogen oxides and ozaone in a temperate deciduos forest and a subartic woodland 1. Measurements and mechanisms, J. Geophys. Res., 101, 12639–12657, 1996.

Musselman, R. C., Lefohn, A. S., Massman, W. J., and Heath, R. L.: A critical review and analysis of the use of exposure- and flux-based ozone indices for predicting vegetation effects, Atmos. Environ., 40, 1869–1888, https://doi.org/10.1016/j.atmosenv.2005.10.064, 2006.

Noormets, A., Chen, J., and Crow, T. R.: Age-Dependent Changes in Ecosystem Carbon Fluxes in Managed Forests in Northern Wisconsin, USA, Ecosystems, 10, 187–203, https://doi.org/10.1007/s10021-007-9018-y, 2007.

Novick, K. A., Ficklin, D. L., Stoy, P. C., Williams, C. A., Bohrer, G., Oishi, A. C., Papuga, S. A., Blanken, P. D., Noormets, A., Sulman, B. N., Scott, R. L., Wang, L., and Phillips, R. P.: The increasing importance of atmospheric demand for ecosystem water and carbon fluxes, Nat. Clim. Change, 6, 1023–1027, https://doi.org/10.1038/nclimate3114, 2016.

Oikawa, P. Y., Jenerette, G. D., Knox, S. H., Sturtevant, C., Verfaillie, J., Dronova, I., Poindexter, C. M., Eichelmann, E., and Baldocchi, D. D.: Evaluation of a hierarchy of models reveals importance of substrate limitation for predicting carbon dioxide and methane exchange in restored wetlands, J. Geophys. Res.-Biogeo., 122, 145–167, https://doi.org/10.1002/2016jg003438, 2017.

Paoletti, E. and Manning, W. J.: Toward a biologically significant and usable standard for ozone that will also protect plants, Environ. Pollut., 150, 85–95, https://doi.org/10.1016/j.envpol.2007.06.037, 2007.

Papale, D., Migliavacca, M., Cremonese, E., Cescatti, A., Alberti, G., Balzarolo, M., Marchesini, L. B., Canfora, E., Casa, R., Duce, P., Facini, O., Galvagno, M., Genesio, L., Gianelle, D., Magliulo, V., Matteucci, G., Montagnani, L., Petrella, F., Pitacco, A., Seufert, G., Spano, D., Stefani, P., Vaccari, F. P., and Valentini, R.: Carbon, water and anergy fluxes of terrestrial ecosystems in Italy, in The Greenhouse Gas Balance of Italy, Springer, Berlin Heidelberg, 11–45, 2015.

Pastorello, G., Agarwal, D., Papale, D., Samak, T., Trotta, C., Ribeca, A., Poindexter, C., Faybishenko, B., Gunter, D., Hollowgrass, R., and Canfora, E.: Observational data patterns for time series data quality assessment, 2014 IEEE 10th Int. Conf. e-Science, 271–278, https://doi.org/10.1109/eScience.2014.45, 2014.

Pastorello, G., Papale, D., Chu, H., Trotta, C., Agarwal, D., Canfora, E., Baldocchi, D., and Torn, M.: A new data set to keep a sharper eye on land-air exchanges, Eos, 98, https://doi.org/10.1029/2017EO071597, 2017.

Plake, D., Stella, P., Moravek, A., Mayer, J. C., Ammann, C., Held, A., and Trebs, I.: Comparison of ozone depo-

sition measured with the dynamic chamber and the eddy covariance method, Agr. Forest Meteorol., 206, 97–112, https://doi.org/10.1016/j.agrformet.2015.02.014, 2015.

Pleijel, H., Danielsson, H., Ojanperä, K., De Temmerman, L., Högy, P., Badiani, M., and Karlsson, P. E.: Relationships between ozone exposure and yield loss in European wheat and potato – A comparison of concentration- and flux-based exposure indices, Atmos. Environ., 38, 2259–2269, https://doi.org/10.1016/j.atmosenv.2003.09.076, 2004.

Pleijel, H., Danielsson, H., Simpson, D., and Mills, G.: Have ozone effects on carbon sequestration been overestimated? A new biomass response function for wheat, Biogeosciences, 11, 4521–4528, https://doi.org/10.5194/bg-11-4521-2014, 2014.

Pilegaard, K., Ibrom, A., Courtney, M. S., Hummelshøj, P., and Jensen, N. O.: Increasing net CO_2 uptake by a Danish beech forest during the period from 1996 to 2009, Agr. Forest Meteorol., 151, 934–946, https://doi.org/10.1016/j.agrformet.2011.02.013, 2011.

Post, H., Franssen, H. J. H., Graf, A., Schmidt, M., and Vereecken, H.: Uncertainty analysis of eddy covariance CO_2 flux measurements for different EC tower distances using an extended two-tower approach, Biogeosciences, 12, 1205–1221, https://doi.org/10.5194/bg-12-1205-2015, 2015.

Powell, T. L., Bracho, R., Li, J., Dore, S., Hinkle, C. R., and Drake, B. G.: Environmental controls over net ecosystem carbon exchange of scrub oak in central Florida, Agr. Forest Meteorol., 141, 19–34, https://doi.org/10.1016/j.agrformet.2006.09.002, 2006.

Prescher, A.-K., Grünwald, T., and Bernhofer, C.: Land use regulates carbon budgets in eastern Germany: From NEE to NBP, Agr. Forest Meteorol., 150, 1016–1025, https://doi.org/10.1016/j.agrformet.2010.03.008, 2010.

Rambal, S., Joffre, R., Ourcival, J. M., Cavender-Bares, J., and Rocheteau, A.: The growth respiration component in eddy CO_2 flux from a Quercus ilex mediterranean forest, Glob. Change Biol., 10, 1460–1469, https://doi.org/10.1111/j.1365-2486.2004.00819.x, 2004.

Rannik, Ü., Mammarella, I., Keronen, P., and Vesala, T.: Vertical advection and nocturnal deposition of ozone over a boreal pine forest, Atmos. Chem. Phys., 9, 2089–2095, https://doi.org/10.5194/acp-9-2089-2009, 2009.

Rannik, Ü., Altimir, N., Mammarella, I., Bäck, J., Rinne, J., Ruuskanen, T. M., Hari, P., Vesala, T., and Kulmala, M.: Ozone deposition into a boreal forest over a decade of observations: Evaluating deposition partitioning and driving variables, Atmos. Chem. Phys., 12, 12165–12182, https://doi.org/10.5194/acp-12-12165-2012, 2012.

Raz-Yaseef, N., Billesbach, D. P., Fischer, M. L., Biraud, S. C., Gunter, S. A., Bradford, J. A., and Torn, M. S.: Vulnerability of crops and native grasses to summer drying in the U.S. Southern Great Plains, Agr. Ecosyst. Environ., 213, 209–218, https://doi.org/10.1016/j.agee.2015.07.021, 2015.

Reda, I. and Andreas, A.: Solar position algorithm for solar radiation applications, Sol. Energ., 76, 577–589, https://doi.org/10.1016/j.solener.2003.12.003, 2004.

Reich, P. B.: Quantifying plant response to ozone: A unifying theory, Tree Physiol., 3, 63–91, https://doi.org/10.1093/treephys/3.1.63, 1987.

Reich, P. B. and Amundson, R. G.: Ambient levels of ozone reduce net photosynthesis in tree and crop species, Science, 230, 566–570, 1985.

Reich, P. B. and Lassoie, J. P.: Effects of low level O_3 exposure on leaf diffusive conductance and water-use efficiency in hybrid poplar, Plant. Cell Environ., 7, 661–668, https://doi.org/10.1111/1365-3040.ep11571645, 1984.

Reichle, R., Draper, C., Liu, Q., Girotto, M., Mahanama, S., Koster, R., and Lannoy, G.: Assessment of MERRA-2 Land Surface Hydrology Estimates, Am. Meteorol. Soc. J. Clim., 30, 2937–2960, https://doi.org/10.1175/JCLI-D-16-0720.1, 2017.

Reichstein, M., Falge, E., Baldocchi, D., Papale, D., Aubinet, M., Berbigier, P., Bernhofer, C., Buchmann, N., Gilmanov, T., Granier, A., Grünwald, T., Havránková, K., Ilvesniemi, H., Janous, D., Knohl, A., Laurila, T., Lohila, A., Loustau, D., Matteucci, G., Meyers, T., Miglietta, F., Ourcival, J. M., Pumpanen, J., Rambal, S., Rotenberg, E., Sanz, M., Tenhunen, J., Seufert, G., Vaccari, F., Vesala, T., Yakir, D., and Valentini, R.: On the separation of net ecosystem exchange into assimilation and ecosystem respiration: Review and improved algorithm, Glob. Change Biol., 11, 1424–1439, https://doi.org/10.1111/j.1365-2486.2005.001002.x, 2005.

Reverter, B. R., Sánchez-Cañete, E. P., Resco, V., Serrano-Ortiz, P., Oyonarte, C., and Kowalski, A. S.: Analyzing the major drivers of NEE in a Mediterranean alpine shrubland, Biogeosciences, 7, 2601–2611, https://doi.org/10.5194/bg-7-2601-2010, 2010.

Rey, A., Pegoraro, E., Tedeschi, V., Parri, I. De, Jarvis, P. G., and Valentini, R.: Annual variation in soil respiration and its components in a coppice oak forest in Central Italy, Glob. Change Biol., 8, 851–866, https://doi.org/10.1046/j.1365-2486.2002.00521.x, 2002.

Ruehr, N. K., Martin, J. G., and Law, B. E.: Effects of water availability on carbon and water exchange in a young ponderosa pine forest: Above- and belowground responses, Agr. Forest Meteorol., 164, 136–148, https://doi.org/10.1016/j.agrformet.2012.05.015, 2012.

Sabbatini, S., Arriga, N., Bertolini, T., Castaldi, S., Chiti, T., Consalvo, C., Djomo, S. N., Gioli, B., Matteucci, G., and Papale, D.: Greenhouse gas balance of cropland conversion to bioenergy poplar short-rotation coppice, Biogeosciences, 13, 95–113, https://doi.org/10.5194/bg-13-95-2016, 2016.

Schmidt, M., Reichenau, T. G., Fiener, P., and Schneider, K.: The carbon budget of a winter wheat field: An eddy covariance analysis of seasonal and inter-annual variability, Agr. Forest Meteorol., 165, 114–126, https://doi.org/10.1016/j.agrformet.2012.05.012, 2012.

Schnell, J. L., Holmes, C. D., Jangam, A., and Prather, M. J.: Skill in forecasting extreme ozone pollution episodes with a global atmospheric chemistry model, Atmos. Chem. Phys., 14, 7721–7739, https://doi.org/10.5194/acp-14-7721-2014, 2014.

Schwede, D., Zhang, L., Vet, R., and Lear, G.: An intercomparison of the deposition models used in the CASTNET and CAPMoN networks, Atmos. Environ., 45, 1337–1346, https://doi.org/10.1016/j.atmosenv.2010.11.050, 2011.

Scott, R. L. and Biederman, J. A.: Partitioning evapotranspiration using long-term carbon dioxide and water vapor fluxes, Geophys. Res. Lett., 44, 6833–6840, https://doi.org/10.1002/2017GL074324, 2017.

Scott, R. L., Jenerette, G. D., Potts, D. L., and Huxman, T. E.: Effects of seasonal drought on net carbon dioxide exchange from a woody-plant-encroached semiarid grassland, J. Geophys. Res., 114, G04004, https://doi.org/10.1029/2008jg000900, 2009.

Scott, R. L., Hamerlynck, E. P., Jenerette, G. D., Moran, M. S., and Barron-Gafford, G. A.: Carbon dioxide exchange in a semidesert grassland through drought-induced vegetation change, J. Geophys. Res., 115, G03026, https://doi.org/10.1029/2010jg001348, 2010.

Scott, R. L., Biederman, J. A., Hamerlynck, E. P., and Barron-Gafford, G. A.: The carbon balance pivot point of southwestern U.S. semiarid ecosystems: Insights from the 21st century drought, J. Geophys. Res.-Biogeo., 120, 2612–2624, https://doi.org/10.1002/2015jg003181, 2015.

Seabold, S. and Perktold, J.: Statsmodels: econometric and statistical modeling with Python, in: Proceedings of the 9th Python in Science Conference, 57–61, 2010.

Sen, P. K.: Estimates of the regression coefficient based on Kendall's tau, J. Am. Stat. Assoc., 63, 1379–1389, https://doi.org/10.1080/01621459.1968.10480934, 1968.

Silva, S. J. and Heald, C. L.: Investigating dry deposition of ozone to vegetation, J. Geophys. Res.-Atmos., 123, 559–573, https://doi.org/10.1002/2017JD027278, 2018.

Sitch, S., Cox, P. M., Collins, W. J., and Huntingford, C.: Indirect radiative forcing of climate change through ozone effects on the land-carbon sink, Nature, 448, 791–794, https://doi.org/10.1038/nature06059, 2007.

Stella, P., Personne, E., Loubet, B., Lamaud, E., Ceschia, E., Béziat, P., Bonnefond, J. M., Irvine, M., Keravec, P., Mascher, N., and Cellier, P.: Predicting and partitioning ozone fluxes to maize crops from sowing to harvest: The Surfatm-O_3 model, Biogeosciences, 8, 2869–2886, https://doi.org/10.5194/bg-8-2869-2011, 2011a.

Stella, P., Loubet, B., Lamaud, E., Laville, P., and Cellier, P.: Ozone deposition onto bare soil?: A new parameterization, Agr. Forest Meteorol., 151, 669–681, https://doi.org/10.1016/j.agrformet.2011.01.015, 2011b.

Stella, P., Kortner, M., Ammann, C., Foken, T., Meixner, F. X., and Trebs, I.: Measurements of nitrogen oxides and ozone fluxes by eddy covariance at a meadow: Evidence for an internal leaf resistance to NO_2, Biogeosciences, 10, 5997–6017, https://doi.org/10.5194/bg-10-5997-2013, 2013.

Sulman, B. N., Desai, A. R., Cook, B. D., Saliendra, N., and Mackay, D. S.: Contrasting carbon dioxide fluxes between a drying shrub wetland in Northern Wisconsin, USA, and nearby forests, Biogeosciences, 6, 1115–1126, https://doi.org/10.5194/bg-6-1115-2009, 2009.

Tai, A. P. K., Martin, M. V., and Heald, C. L.: Threat to future global food security from climate change and ozone air pollution, Nat. Clim. Change, 4, 817–821, https://doi.org/10.1038/nclimate2317, 2014.

Taylor, J. R.: An Introduction to Error Analysis, University Science Books, Sausalito, 1–327, 1997.

Tedeschi, V., Ret, A., Manca, G., Valentini, R., Jarvis, P. G., and Borghetti, M.: Soil respiration in a Mediterranean oak forest at different developmental stages after coppicing, Glob. Change Biol., 12, 110–121, https://doi.org/10.1111/j.1365-2486.2005.01081.x, 2006.

Thum, T., Aalto, T., Laurila, T., Aurela, M., Kolari, P., and Hari, P.: Parametrization of two photosynthesis models at the canopy scale in a northern boreal Scots pine forest, Tellus B, 59, 874–890, https://doi.org/10.3402/tellusb.v59i5.17066, 2007.

UNECE: Revised manual on methodologies and criteria for mapping critical levels/loads and geographical areas where they are exceeded, in: UNECE Convention on Long-range Transboundary Air Pollution, 2004.

Urbanski, S., Barford, C., Wofsy, S., Kucharik, C., Pyle, E., Budney, J., McKain, K., Fitzjarrald, D., Czikowsky, M., and Munger, J. W.: Factors controlling CO_2 exchange on timescales from hourly to decadal at Harvard Forest, J. Geophys. Res., 112, G02020, https://doi.org/10.1029/2006jg000293, 2007.

Valentini, R., Angelis, P., Matteucci, G., Monaco, R., Dore, S., and Mucnozza, G. E. S.: Seasonal net carbon dioxide exchange of a beech forest with the atmosphere, Glob. Change Biol., 2, 199–207, https://doi.org/10.1111/j.1365-2486.1996.tb00072.x, 1996.

Van Dingenen, R., Dentener, F. J., Raes, F., Krol, M. C., Emberson, L., and Cofala, J.: The global impact of ozone on agricultural crop yields under current and future air quality legislation, Atmos. Environ., 43, 604–618, https://doi.org/10.1016/j.atmosenv.2008.10.033, 2009.

Verma, S. B., Dobermann, A., Cassman, K. G., Walters, D. T., Knops, J. M., Arkebauer, T. J., Suyker, A. E., Burba, G. G., Amos, B., Yang, H., Ginting, D., Hubbard, K. G., Gitelson, A. A., and Walter-Shea, E. A.: Annual carbon dioxide exchange in irrigated and rainfed maize-based agroecosystems, Agr. Forest Meteorol., 131, 77–96, https://doi.org/10.1016/j.agrformet.2005.05.003, 2005.

Vitale, L., Tommasi, P. Di, D'Urso, G., and Magliulo, V.: The response of ecosystem carbon fluxes to LAI and environmental drivers in a maize crop grown in two contrasting seasons, Int. J. Biometeorol., 60, 411–420, https://doi.org/10.1007/s00484-015-1038-2, 2015.

Vuichard, N. and Papale, D.: Filling the gaps in meteorological continuous data measured at FLUXNET sites with ERA-Interim reanalysis, Earth Syst. Sci. Data, 7, 157–171, https://doi.org/10.5194/essd-7-157-2015, 2015.

Van Der Walt, S., Colbert, S. C., and Varoquaux, G.: The NumPy array: A structure for efficient numerical computation, Comput. Sci. Eng., 13, 22–30, https://doi.org/10.1109/MCSE.2011.37, 2011.

Wang, L., Good, S. P., and Caylor, K. K.: Global synthesis of vegetation control on evapotranspiration partitioning, Geophys. Res. Lett., 41, 6753–6757, https://doi.org/10.1002/2014GL061439, 2014.

Warton, D. I., Wright, I. J., Falster, D. S., and Westoby, M.: Bivariate line-fitting methods for allometry, Biol. Rev., 81, 259–291, https://doi.org/10.1017/S1464793106007007, 2006.

Weaver, J. E. and Bruner, W. E.: Root development of vegetable crops, McGraw-Hill Book Company, Inc., Lincoln, Nebraska, 1927.

Wesely, M. L. and Hicks, B. B.: Some factors that affect the deposition rates of sulfur dioxide and similar gases on vegetation, J. Air Pollut. Control Assoc., 27, 1110–1116, https://doi.org/10.1080/00022470.1977.10470534, 1977.

Wesley, M. L.: Parametrization of surface resistance to gaseous dry deposition in regional-scale numerical model, Atmos. Environ., 23, 1293–1304, 1989.

Wittig, V. E., Ainsworth, E. A., and Long, S. P.: To what extent do current and projected increases in surface ozone affect photosynthesis and stomatal conductance of trees? A meta-analytic review of the last 3 decades of experiments, Plant Cell Environ., 30, 1150–1162, https://doi.org/10.1111/j.1365-3040.2007.01717.x, 2007.

Wittig, V. E., Ainsworth, E. A., Naidu, S. L., Karnosky, D. F., and Long, S. P.: Quantifying the impact of current and future tropospheric ozone on tree biomass, growth, physiology and biochemistry: A quantitative meta-analysis, Glob. Change Biol., 15, 396–424, https://doi.org/10.1111/j.1365-2486.2008.01774.x, 2009.

Wohlfahrt, G., Hammerle, A., Haslwanter, A., Bahn, M., Tappeiner, U., and Cernusca, A.: Seasonal and inter-annual variability of the net ecosystem CO_2 exchange of a temperate mountain grassland: Effects of weather and management, J. Geophys. Res., 113, D08110, https://doi.org/10.1029/2007jd009286, 2008.

Wolfe, G. M., Thornton, J. A., Mckay, M., and Goldstein, A. H.: Forest-atmosphere exchange of ozone?: sensitivity to very reactive biogenic VOC emissions and implications for in-canopy photochemistry, Atmos. Chem. Phys., 11, 7875–7891, https://doi.org/10.5194/acp-11-7875-2011, 2011.

Wu, S., Mickley, L. J., Jacob, D. J., Logan, J. A., Yantosca, R. M., and Rind, D.: Why are there large differences between models in global budgets of tropospheric ozone?, J. Geophys. Res.-Atmos., 112, D05302, https://doi.org/10.1029/2006JD007801, 2007.

Wu, Z., Schwede, D. B., Vet, R., Walker, J. T., Shaw, M., Staebler, R., and Zhang, L.: Evaluation and intercomparison of five North American dry deposition algorithms at a mixed forest site, J. Adv. Model. Earth Syst., 10, 1571–1586, https://doi.org/10.1029/2017MS001231, 2018.

Young, P. J., Archibald, A. T., Bowman, K. W., Lamarque, J.-F., Naik, V., Stevenson, D. S., Tilmes, S., Voulgarakis, A., Wild, O., Bergmann, D., Cameron-Smith, P., Cionni, I., Collins, W. J., Dalsøren, S. B., Doherty, R. M., Eyring, V., Faluvegi, G., Horowitz, L. W., Josse, B., Lee, Y. H., MacKenzie, I. A., Nagashima, T., Plummer, D. A., Righi, M., Rumbold, S. T., Skeie, R. B., Shindell, D. T., Strode, S. A., Sudo, K., Szopa, S., and Zeng, G.: Pre-industrial to end 21st century projections of tropospheric ozone from the Atmospheric Chemistry and Climate Model Intercomparison Project (ACCMIP), Atmos. Chem. Phys., 13, 2063–2090, https://doi.org/10.5194/acp-13-2063-2013, 2013.

Yue, X. and Unger, N.: Ozone vegetation damage effects on gross primary productivity in the United States, Atmos. Chem. Phys., 14, 9137–9153, https://doi.org/10.5194/acp-14-9137-2014, 2014.

Yue, X., Keenan, T. F., Munger, W., and Unger, N.: Limited effect of ozone reductions on the 20-year photosynthesis trend at Harvard forest, Glob. Change Biol., 22, 3750–3759, https://doi.org/10.1111/gcb.13300, 2016.

Zeller, K. F. and Nikolov, N. T.: Quantifying simultaneous fluxes of ozone, carbon dioxide and water vapor above a subalpine forest ecosystem, Environ. Pollut., 107, 1–20, 2000.

Zhang, L., Brook, J. R. and Vet, R.: On ozone dry deposition – With emphasis on non-stomatal uptake and wet canopies, Atmos. Environ., 36, 4787–4799, https://doi.org/10.1016/S1352-2310(02)00567-8, 2002.

Zhang, L., Brook, J. R., and Vet, R.: A revised parameterization for gaseous dry deposition in air-quality models, Atmos. Chem. Phys., 3, 2067–2082, https://doi.org/10.5194/acp-3-2067-2003, 2003.

Zhou, S., Yu, B., Huang, Y., and Wang, G.: Partitioning evapotranspiration based on the concept of underlying water use efficiency, Water Resour. Res., 52, 1160–1175, https://doi.org/10.1002/2015WR017766, 2016.

Zielis, S., Etzold, S., Zweifel, R., Eugster, W., Haeni, M., and Buchmann, N.: NEP of a Swiss subalpine forest is significantly driven not only by current but also by previous years weather, Biogeosciences, 11, 1627–1635, https://doi.org/10.5194/bg-11-1627-2014, 2014.

Zona, D., Gioli, B., Fares, S., De Groote, T., Pilegaard, K., Ibrom, A., and Ceulemans, R.: Environmental controls on ozone fluxes in a poplar plantation in Western Europe, Environ. Pollut., 184, 201–210, https://doi.org/10.1016/j.envpol.2013.08.032, 2014.

Supplement of Biogeosciences, 15, 5395–5413, 2018
https://doi.org/10.5194/bg-15-5395-2018-supplement

Biogeosciences Open Access EGU

Supplement of

Synthetic ozone deposition and stomatal uptake at flux tower sites

Jason A. Ducker et al.

Correspondence to: Jason A. Ducker (jad10d@my.fsu.edu)

S1 Calculation of stomatal conductance and deposition velocity

Several methods for calculating stomatal conductance and O_3 deposition velocity from eddy covariance measurements are found in literature (e.g. Wesely and Hicks, 1977; Gerosa et al., 2005; Fares et al., 2010). While we follow the same general approach, we present the methods here for completeness and to point out some particular choices we have made. These expressions are used in Eqs. 1-3. The required input variables are O_3 mole fraction (mol mol^{-1}), temperature (K), pressure (Pa), specific humidity (kg kg^{-1}), friction velocity (m s^{-1}), sensible and latent heat fluxes (W m^{-2}), canopy height (m), and leaf area index (m^2 m^{-2}).

The aerodynamic and quasi-laminar layer resistances are calculated from measurements of momentum flux using the Monin-Obukhov similarity relations. For heat, O_3, and other gases, the aerodynamic resistance (r_a, s m^{-1}) is (Foken, 2017, pp. 219-223)

$$r_a = \frac{1}{k u_*}\left[\ln\left(\frac{z-d}{z_0}\right) - \psi_H\left(\frac{z-d}{L}\right) + \psi_H\left(\frac{z_0}{L}\right)\right] \quad \text{(A1)}$$

where r_a is evaluated at height z, u_* is the friction velocity, z_0 (m) is the roughness length for momentum, d (m) is the displacement height, $k = 0.4$ is the von Karman constant, $\psi_H(\zeta)$ is the stability function for sensible heat discussed below, and L is the Obukhov length (m). The roughness and displacement heights are $z_0 = 0.1 z_c$ and $d = 0.7 z_c$, respectively, where z_c is the canopy height specific to each site (http://fluxnet.fluxdata.org/sites/site-summary/, accessed 24 February 2017). Since canopy heights are not specified for croplands or grasslands in this database, we use a constant canopy height of 1 m for grasslands and typical crop-specific heights for each agricultural site (Weaver and Bruner, 1927). The stability function is (Foken, 2017, pp. 54-62; Högström, 1988)

$$\psi_H(\zeta) = \begin{cases} 2\ln\left(\dfrac{1 + 0.95(1 - 11.6\zeta)^{1/2}}{2}\right) & \text{for } \zeta < 0 \\ 1 - \left(1 + \dfrac{2}{3}\zeta\right)^{\frac{3}{2}} - b_1\left(\zeta - \dfrac{b_2}{b_3}\right)\exp(-b_3\zeta) - \dfrac{b_1 b_2}{b_3} & \text{for } \zeta \geq 0 \end{cases} \quad \text{(A2)}$$

where $b_1 = 0.667$, $b_2 = 5$, and $b_3 = 0.35$. The form above is appropriate for strongly stable conditions ($(z-d)/L = \zeta > 1$), which occur frequently in the FLUXNET2015 data, as well weak stability (Beljaars and Holtslag, 1991).

The Obukhov length is (Foken, 2017, pp. 54-62)

$$L = -\frac{u_*^3 \theta_v}{k g(\overline{w'\theta_v'})} \quad \text{(A3)}$$

where θ_v is virtual potential temperature, $\overline{w'\theta_v'}$ is the vertical flux of virtual potential temperature or buoyancy at the surface, and g is acceleration due to gravity. For calculations, we expand θ_v and $\overline{w'\theta_v'}$ in terms of measured quantities so

$$L = -\frac{u_*^3 c_p \rho \theta (1 + 0.61q)}{kg\big(H(1 + 0.61q) + 0.61 c_p \theta E\big)} \tag{A4}$$

where c_p is specific heat capacity of air (J kg^{-1} K^{-1}), ρ is the mass density of air (kg m^{-3}), θ is potential temperature (K), q is specific humidity (kg kg^{-1}), H is the surface sensible heat flux (W m^{-2}), and E is the surface moisture flux (kg m^{-2} s^{-1}). H and E are defined positive for upward fluxes.

The quasi-laminar layer resistance for O_3 and H_2O is (Foken, 2017, pp. 219-223)

$$r_b = \frac{2}{k u_*}\left(\frac{\mathrm{Sc}}{\mathrm{Pr}}\right)^{2/3}, \tag{A5}$$

where Sc = ν/D is the Schmidt number, which is the ratio of kinematic viscosity of air (ν) to the molecular diffusivity of the gas in air (D), and Pr = ν/D_H is the Prandtl number, which involves the thermal diffusivity (D_H). The conductance for heat is the same as Eq. A5, but uses the thermal diffusivity of air in place of molecular diffusivity.

We calculate stomatal resistance and conductance from the evaporative-resistance form of the Penman-Monteith equation (Monteith, 1981; Gerosa et al., 2007). For water vapor,

$$g_{s,w}^{-1} = r_{s,w} = \frac{\varepsilon \rho \big(e_s(T_f) - e\big)}{pE} - \big(r_a + r_{b,w}\big) \tag{A6}$$

where ε = 0.622 is the mass ratio of H_2O and dry air, p is the air pressure, $e_s(T_f)$ is the saturation vapor pressure at the transpiring leaf surface with temperature T_f, e is vapor pressure at the flux measurement height, and $r_{b,w}$ is the quasi-laminar layer resistance to water vapor (Eq. A5). Leaf temperature is not a standard FLUXNET2015 variable, but it can be estimated from sensible heat flux using surface energy balance (Gerosa et al., 2007):

$$T_f = T + \frac{H}{c_p \rho}\big(r_a + r_{b,H}\big) \tag{A7}$$

where T is the air temperature at the measurement height and $r_{b,H}$ is the quasi-laminar layer resistance to heat (Eq. A5). We initially inverted Monteith's (1981) original equation for evapotranspiration (Eq. 4 in Gerosa et al., 2007) in place of Eq. A6, but the resulting $g_{s,w}$ estimates were much more noisy. Although the forms are analytically equivalent (Gerosa et al., 2007), inverting the evaporative-resistance form is numerically preferable because it avoids subtractive terms that amplify relative errors and it more accurately treats temperature and pressure effects, particularly the non-linearity in the saturation vapor pressure.

The stomatal conductance of O_3 is less than water vapor due to its greater molar mass and diffusion against the net gas flow out of the stomatal pore (Marrero and Mason, 1972), so

$$g_s = 0.6\, g_{s,w}. \tag{A8}$$

In all equations, we include the temperature and pressure dependences of ρ, c_p, v, D, D_H, and latent heat of vaporization and also the humidity dependence of ρ, c_p, and D_H using expressions from Jacobson (2005).

S2 Propagation of uncertainty

We estimate uncertainties in all derived quantities using standard techniques for propagation of errors (e.g. Taylor, 1997, pp. 73-77). In the following section, f is a function that depends on variables $x_1, x_2, \ldots x_n$ that each have uncertainties $\sigma_{x_1}, \sigma_{x_2}, \ldots \sigma_{x_n}$. The standard error ($\sigma_f$) in $f(x_1, x_2, \ldots x_n)$ at time *i* is approximately

$$\sigma_{f,i}^2 = \sum_{j=1}^{n} \left(\frac{\partial f_i}{\partial x_j} \right)^2 \sigma_{x_j,i}^2 . \quad \text{(B1)}$$

This form neglects covariance between the measurement errors, which is unknown in our case, and is most accurate when $\sigma_{x_j} \ll x_j$. We use centered finite differences to calculate numerical derivatives through all equations.

The propagation of errors reveals that $F_{\mathrm{s,O_3}}^{\mathrm{syn}}$ and other quantities have errors or uncertainties that vary widely from hour to hour. Daily and monthly averages should account for the varying confidence in each value in the average (e.g. Taylor, 1997, pp. 173-177). For values f_i that are from a single distribution, but have different uncertainties $\sigma_{f,i}$, the maximum likelihood estimate of f is

$$\bar{f} = \left(\sum_{i=1}^{m} w_i f_i \right) \left(\sum_{i=1}^{m} w_i \right)^{-1} ; \qquad w_i = {\sigma_{f,i}}^{-2}. \quad \text{(B2)}$$

The weights w_i reflect the confidence in value f_i and the summation is carried out over all times *m* within the desired averaging period. The standard error of $\bar{f}$ is

$$\sigma_{\bar{f}} = \left(\sum_{i=1}^{m} w_i \right)^{-\frac{1}{2}} . \quad \text{(B3)}$$

For averaging across times when *f* is expected to change, as during different hours of the day, an unweighted average is more appropriate

$$\bar{f} = \frac{1}{m} \sum_{i=1}^{m} f_i \quad \text{(B4)}$$

and the standard error of $\bar{f}$, given by Eq. B1, simplifies to

$$\sigma_{\bar{f}} = \left(\frac{1}{m^2} \sum_{i=1}^{m} \sigma_{f,i}^2 \right)^{\frac{1}{2}} . \quad \text{(B5)}$$

S3 Stomatal and non-stomatal O_3 deposition at Harvard Forest

Our estimate of the non-stomatal fraction of O_3 deposition at Harvard Forest (mean 8%, range –33 to 34%; Sect. 3.2) is smaller than was previously reported at that site (mean 40%, range 20-60%; Clifton et al., 2017). The main reason for the different results is the re-calibration of the water vapor fluxes in this work, which is described in Sect. 2.2. Here, we show how other differences between our analysis and that of Clifton et al. (2017) affect the estimate of non-stomatal fraction of O_3 deposition at Harvard Forest. Using our gap-filled data, the mean estimate of the non-stomatal fraction of O_3 deposition at Harvard Forest does not change but the range slightly increases (8%, range –36 to 38%). With uncorrected water vapor fluxes, our estimate would be 51% (range: 32% to 63%). If we also ignore the propagated uncertainty, which varies from hour to hour, and calculate averages with equal weight (i.e. equal uncertainty) for each time interval, as Clifton et al. did, then we would estimate 53% (range: 34% to 66%). If we also use data filtering criteria from Clifton et al. (i.e. remove 3σ outliers of v_d and g_s, but no filtering for precipitation and high relative humidity), then we would estimate 48% (range: 28% to 61%). Finally, if we also restrict our averages to 9am-3pm, as Clifton et al. did, instead of all daylight data, then we would estimate 45% (range: 25% to 60%). This final estimate is very close to the method and value reported by Clifton et al. (2017). The remaining small differences are probably due to Clifton et al. including 1992 in their analysis and differences in the form of the Penman-Monteith and stability functions. Since the re-calibration of water vapor fluxes (Sect. 2.2) is an improvement in this work and the main reason for our results differing from Clifton et al. (2017), our estimates of small non-stomatal fraction O_3 deposition at Harvard Forest appear to be most reliable estimate for this site.

121 Table S1. Description of FLUXNET2015 Tier 1 sites used in SynFlux.
122

Site name	PFT[1]	Lat[2]	Lon[3]	Clim[4]	Period	References[5]
AT-Neu	GRA	47.1167	11.3175	Unk	2002-2012	(Wohlfahrt et al., 2008)
BE-Bra	MF	51.3092	4.5206	Unk	1996-2014	(Carrara et al., 2004)
BE-Lon	CRO	50.5516	4.7461	Cfb	2004-2014	(Moureaux et al., 2006)
BE-Vie	MF	50.3051	5.9981	Cfb	1996-2014	(Aubinet et al., 2001)
CH-Cha	GRA	47.2102	8.4104	Unk	2005-2014	(Merbold et al., 2014)
CH-Dav	ENF	46.8153	9.8559	Unk	1997-2014	(Zielis et al., 2014)
CH-Fru	GRA	47.1158	8.5378	Unk	2005-2014	(Imer et al., 2013)
CH-Lae	MF	47.4781	8.3650	Unk	2004-2014	(Etzold et al., 2011)
CH-Oe1	GRA	47.2858	7.7319	Unk	2002-2008	(Ammann et al., 2009)
CH-Oe2	CRO	47.2863	7.7343	Unk	2004-2014	(Dietiker et al., 2010)
CZ-BK1	ENF	49.5021	18.5369	Unk	2004-2008	(Acosta et al., 2013)
CZ-BK2	GRA	49.4944	18.5429	Unk	2004-2006	–
CZ-wet	WET	49.0247	14.7704	Unk	2006-2014	(Dûsek et al., 2012)
DE-Akm	WET	53.8662	13.6834	Cfb	2009-2014	–
DE-Geb	CRO	51.1001	10.9143	Unk	2001-2014	(Anthoni et al., 2004)
DE-Gri	GRA	50.9500	13.5126	Cfb	2004-2014	(Prescher et al., 2010a)
DE-Hai	DBF	51.0792	10.4530	Unk	2000-2012	(Knohl et al., 2003)
DE-Kli	CRO	50.8931	13.5224	Cfb	2004-2014	(Prescher et al., 2010)
DE-Lkb	ENF	49.0996	13.3047	Unk	2009-2013	(Lindauer et al., 2014)
DE-Obe	ENF	50.7867	13.7213	Cfb	2008-2014	–
DE-RuR[6]	GRA	50.6219	6.3041	Unk	2011-2014	(Post et al., 2015)
DE-RuS[6]	CRO	50.8659	6.4472	Cfb	2011-2014	(Mauder et al., 2013)
DE-Seh	CRO	50.8706	6.4497	Unk	2007-2010	(Schmidt et al., 2012)
DE-SfN	WET	47.8064	11.3275	Unk	2012-2014	(Hommeltenberg et al., 2014)
DE-Spw	WET	51.8923	14.0337	Cfb	2010-2014	–
DE-Tha	ENF	50.9624	13.5652	Cfb	1996-2014	(Grünwald and Bernhofer, 2007)
DK-Fou	CRO	56.4842	9.5872	Unk	2005-2005	–
DK-Sor	DBF	55.4859	11.6446	Unk	1996-2014	(Pilegaard et al., 2011)
ES-LgS	OSH	37.0979	-2.9658	Unk	2007-2009	(Reverter et al., 2010)
ES-Ln2	OSH	36.9695	-3.4758	Unk	2009-2009	–
FI-Hyy	ENF	61.8474	24.2948	Unk	1996-2014	(Mammarella et al., 2007)
FI-Jok	CRO	60.8986	23.5135	Unk	2000-2003	(Lohila, 2004)
FI-Lom	WET	67.9972	24.2092	Unk	2007-2009	–
FI-Sod	ENF	67.3619	26.6378	Unk	2001-2014	(Thum et al., 2007)
FR-Fon	DBF	48.4764	2.7801	Cfb	2005-2014	(Delpierre et al., 2015)
FR-Gri	CRO	48.8442	1.9519	Cfb	2004-2013	(Loubet et al., 2011)
FR-LBr	ENF	44.7171	-0.7693	Unk	1996-2008	(Berbigier et al., 2001)
FR-Pue	EBF	43.7414	3.5958	Unk	2000-2014	(Rambal et al., 2004)
IT-BCi	CRO	40.5238	14.9574	Unk	2004-2014	(Vitale et al., 2015)
IT-CA1	DBF	42.3804	12.0266	Unk	2011-2014	(Sabbatini et al., 2016)
IT-CA2	CRO	42.3772	12.0260	Unk	2011-2014	(Sabbatini et al., 2016)
IT-CA3	DBF	42.3800	12.0222	Unk	2011-2014	(Sabbatini et al., 2016)
IT-Col	DBF	41.8494	13.5881	Unk	1996-2014	(Valentini et al., 1996)

IT-Cp2	EBF	41.7043	12.3573	Unk	2012-2014	(Fares et al., 2014)
IT-Cpz	EBF	41.7052	12.3761	Unk	1997-2009	(Garbulsky et al., 2008)
IT-Isp	DBF	45.8126	8.6336	Unk	2013-2014	(Ferréa et al., 2012)
IT-La2	ENF	45.9542	11.2853	Unk	2000-2002	(Marcolla et al., 2003)
IT-Lav	ENF	45.9562	11.2813	Unk	2003-2014	(Marcolla et al., 2003)
IT-MBo	GRA	46.0147	11.0458	Unk	2003-2013	(Marcolla et al., 2011)
IT-Noe	CSH	40.6061	8.1515	Unk	2004-2014	(Papale et al., 2014)
IT-PT1	DBF	45.2009	9.0610	Unk	2002-2004	(Migliavacca et al., 2009)
IT-Ren	ENF	46.5869	11.4337	Unk	1998-2013	(Montagnani et al., 2009)
IT-Ro1	DBF	42.4081	11.9300	Unk	2000-2008	(Rey et al., 2002)
IT-Ro2	DBF	42.3903	11.9209	Unk	2002-2012	(Tedeschi et al., 2006)
IT-SR2	ENF	43.7320	10.2910	Unk	2013-2014	–
IT-SRo	ENF	43.7279	10.2844	Unk	1999-2012	(Chiesi et al., 2005)
IT-Tor	GRA	45.8444	7.5781	Unk	2008-2014	(Galvagno et al., 2013)
NL-Hor	GRA	52.2404	5.0713	Unk	2004-2011	(Jacobs et al., 2007)
NL-Loo	ENF	52.1666	5.7436	Unk	1996-2013	(Dolman et al., 2002)
RU-Fyo	ENF	56.4615	32.9221	Unk	1998-2014	(Kurbatova et al., 2008)
US-AR1	GRA	36.4267	-99.4200	Dsa	2009-2012	(Raz-Yaseef et al., 2015)
US-AR2	GRA	36.6358	-99.5975	Dsa	2009-2012	(Raz-Yaseef et al., 2015)
US-ARb	GRA	35.5497	-98.0402	Cfa	2005-2006	(Raz-Yaseef et al., 2015)
US-ARc	GRA	35.5465	-98.0400	Cfa	2005-2006	(Raz-Yaseef et al., 2015)
US-ARM	CRO	36.6058	-97.4888	Cfa	2003-2012	(Fischer et al., 2007)
US-Blo	ENF	38.8953	-120.6328	Csa	1997-2007	(Goldstein et al., 2000)
US-Cop	GRA	38.0900	-109.3900	Unk	2001-2007	(Bowling et al., 2010)
US-GBT	ENF	41.3658	-106.2397	Dfc	1999-2006	(Zeller and Nikolov, 2000)
US-GLE	ENF	41.3665	-106.2399	Dfc	2004-2014	(Frank et al., 2014)
US-Ha1	DBF	42.5378	-72.1715	Dfb	1991-2012	(Urbanski et al., 2007)
US-KS2	CSH	28.6086	-80.6715	Cwa	2003-2006	(Powell et al., 2006)
US-Los	WET	46.0827	-89.9792	Dfb	2000-2014	(Sulman et al., 2009)
US-Me1	ENF	44.5794	-121.5000	Csb	2004-2005	(Irvine et al., 2007)
US-Me2	ENF	44.4523	-121.5574	Csb	2002-2014	(Irvine et al., 2008)
US-Me6	ENF	44.3233	-121.6078	Csb	2010-2014	(Ruehr et al., 2012)
US-MMS	DBF	39.3232	-86.4131	Cfa	1999-2014	(Dragoni et al., 2011)
US-Myb	WET	38.0498	-121.7651	Csa	2010-2014	(Matthes et al., 2014)
US-Ne1	CRO	41.1651	-96.4766	Dfa	2001-2013	(Verma et al., 2005)
US-Ne2	CRO	41.1649	-96.4701	Dfa	2001-2013	(Verma et al., 2005)
US-Ne3	CRO	41.1797	-96.4397	Dfa	2001-2013	(Verma et al., 2005)
US-NR1	ENF	40.0329	-105.5464	Dfc	1998-2014	(Monson et al., 2002)
US-ORv	WET	40.0201	-83.0183	Cfa	2011-2011	(Morin et al., 2014)
US-PFa	MF	45.9459	-90.2723	Dfb	1995-2014	(Desai et al., 2015)
US-SRG	GRA	31.7894	-110.8277	Bsk	2008-2014	(Scott et al., 2015)
US-SRM	WSA	31.8214	-110.8661	Bsk	2004-2014	(Scott et al., 2009)
US-Syv	MF	46.2420	-89.3477	Dfb	2001-2014	(Desai et al., 2005)
US-Ton	WSA	38.4316	-120.9660	Csa	2001-2014	(Baldocchi et al., 2010)
US-Tw1	WET	38.1074	-121.6469	Csa	2012-2014	(Oikawa et al., 2017)
US-Tw2	CRO	38.1047	-121.6433	Csa	2012-2013	(Knox et al., 2016)

US-Tw3	CRO	38.1159	-121.6467	Csa	2013-2014	(Baldocchi et al., 2015)
US-Tw4	WET	38.1030	-121.6414	Csa	2013-2014	(Baldocchi, 2016)
US-Twt	CRO	38.1087	-121.6530	Csa	2009-2014	(Hatala et al., 2012)
US-UMB	DBF	45.5598	-84.7138	Dfb	2000-2014	(Gough et al., 2013)
US-UMd	DBF	45.5625	-84.6975	Dfb	2007-2014	(Gough et al., 2013)
US-Var	GRA	38.4133	-120.9507	Csa	2000-2014	(Ma et al., 2007)
US-WCr	DBF	45.8059	-90.0799	Dfb	1999-2014	(Cook et al., 2004)
US-Whs	OSH	31.7438	-110.0522	Bsk	2007-2014	(Scott et al., 2015)
US-Wi0	ENF	46.6188	-91.0814	Dfb	2002-2002	(Noormets et al., 2007)
US-Wi3	DBF	46.6347	-91.0987	Dfb	2002-2004	(Noormets et al., 2007)
US-Wi4	ENF	46.7393	-91.1663	Dfb	2002-2005	(Noormets et al., 2007)
US-Wi6	OSH	46.6249	-91.2982	Dfb	2002-2003	(Noormets et al., 2007)
US-Wi9	ENF	46.6188	-91.0814	Dfb	2004-2005	(Noormets et al., 2007)
US-Wkg	GRA	31.7365	-109.9419	Bsk	2004-2014	(Scott et al., 2010)

[1] Plant functional type; see Table 2 for abbreviations.
[2] Positive value indicates north latitude.
[3] Negative value indicates west longitude.
[4]Köppen Climate classification.
[5] "-" indicates that site operators have not provided a reference.
[6] Latent and sensible heat flux uncertainty not reported for this site; 50% uncertainty is assumed.

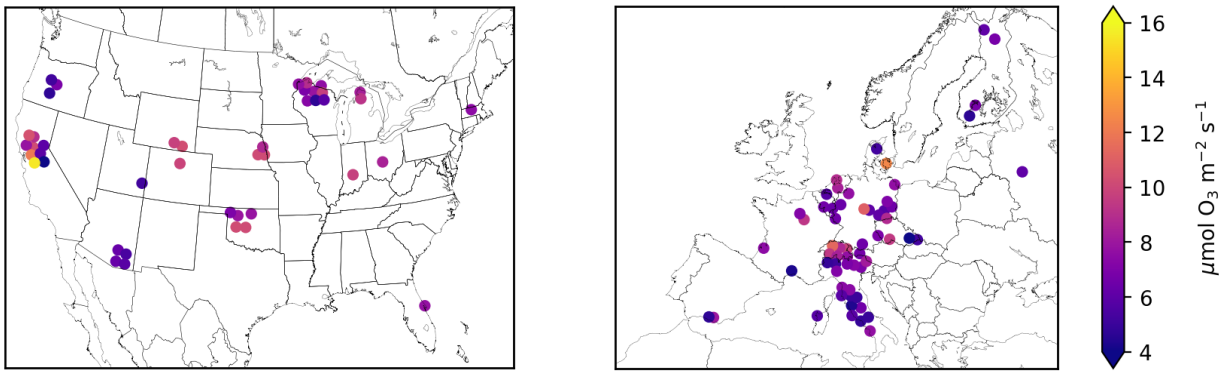

Figure S1. Mean synthetic total O_3 flux ($F_{O_3}^{syn}$, Sect. 2.1) during the daytime growing season at FLUXNET2015 sites in the United States and Europe. Symbols of some sites have been moved slightly to reduce overlap and improve legibility.

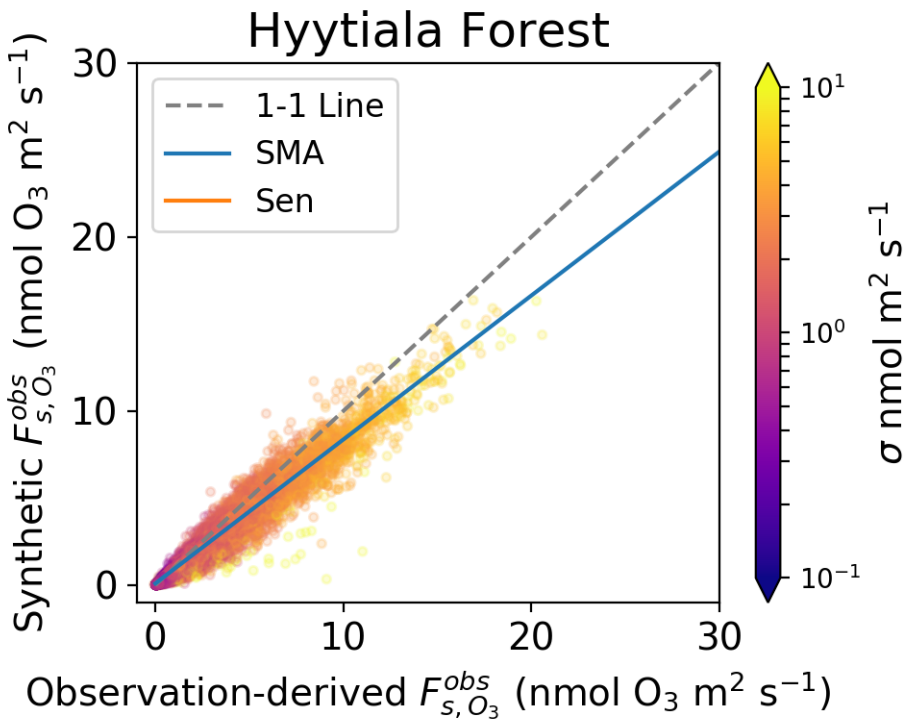

Figure S2. Synthetic and observed stomatal conductance, F_{s,O_3}^{syn}, at Hyytiälä Forest illustrating the errors in half-hourly data. Colors show the standard deviation of each value on a logarithmic scale, as calculated by error propagation.

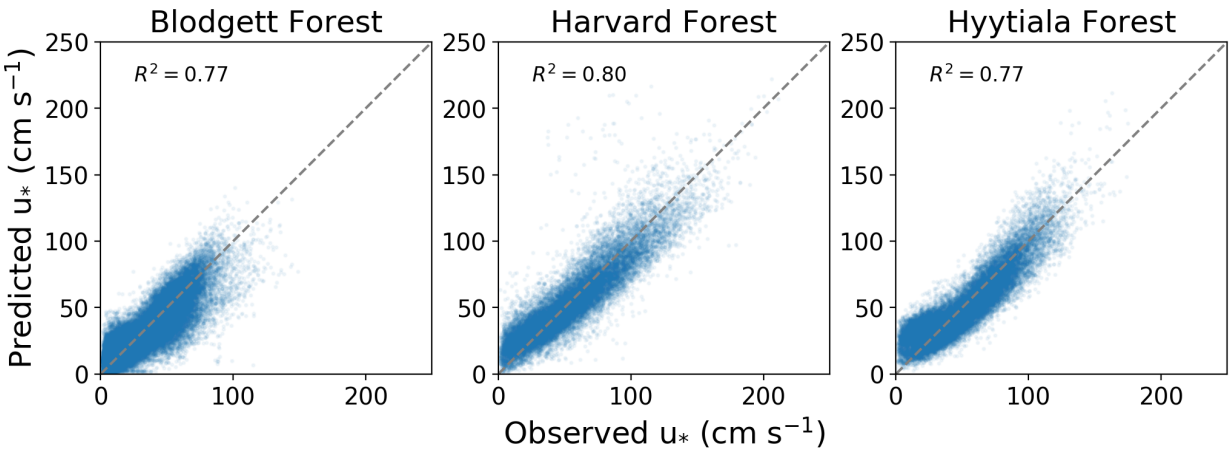

Figure S3. Observed and predicted friction velocity (u_*) from the regression model in Sect 2.3.

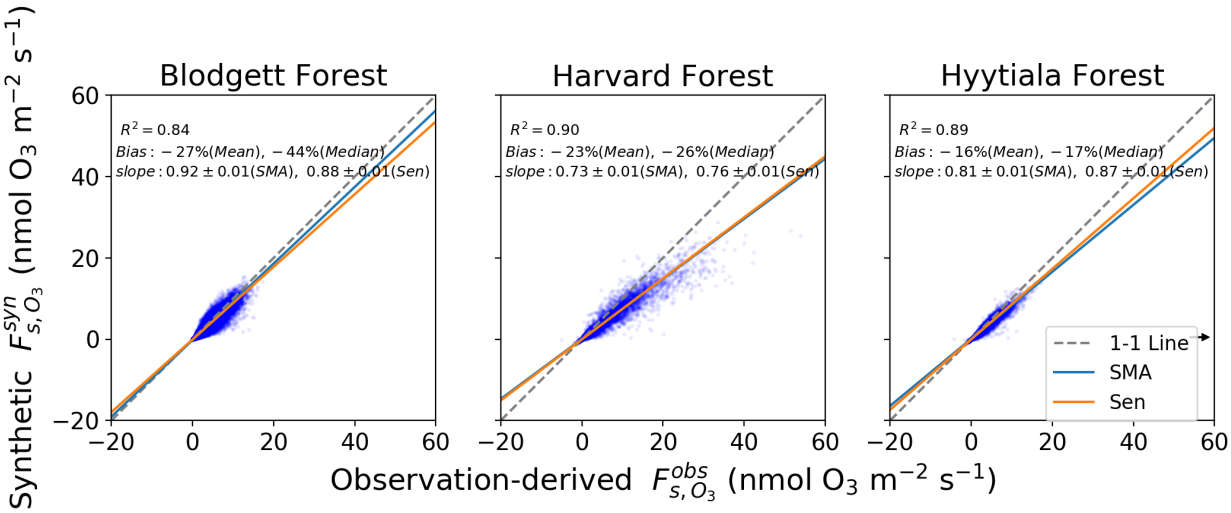

Figure S4. Synthetic and observation-derived half-hourly (hourly at Harvard Forest) stomatal O_3 flux. See Fig. 2 for explanation of lines and inset text.

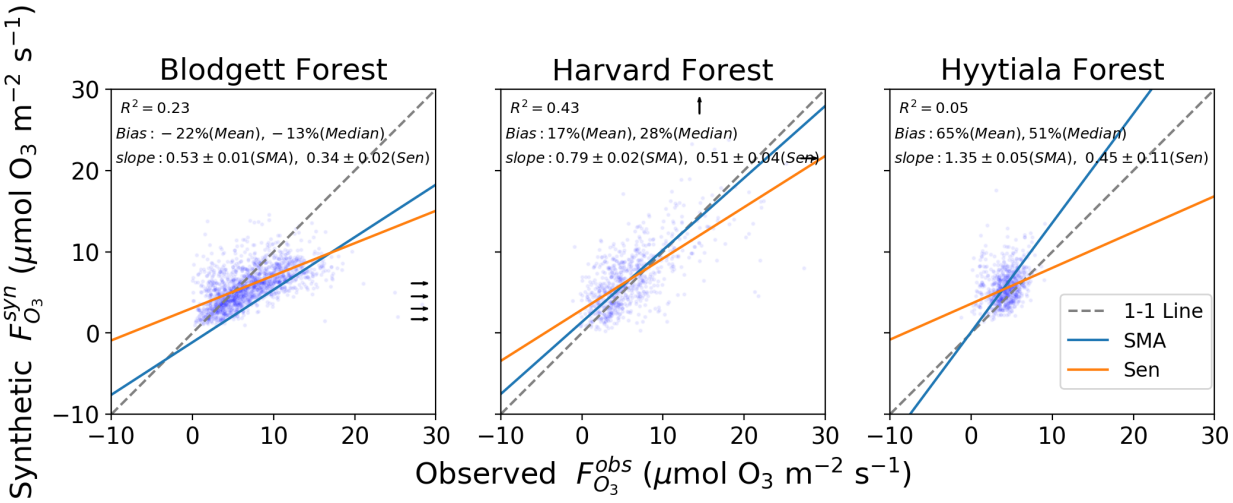

Figure S5. Synthetic and observation-derived daily daytime total O_3 flux ($F_{O_3}^{syn}$, Sect. 2.1). See Sect. 2.1 for explanation of $F_{O_3}^{syn}$ and Fig. 2 for explanation of lines and inset text.

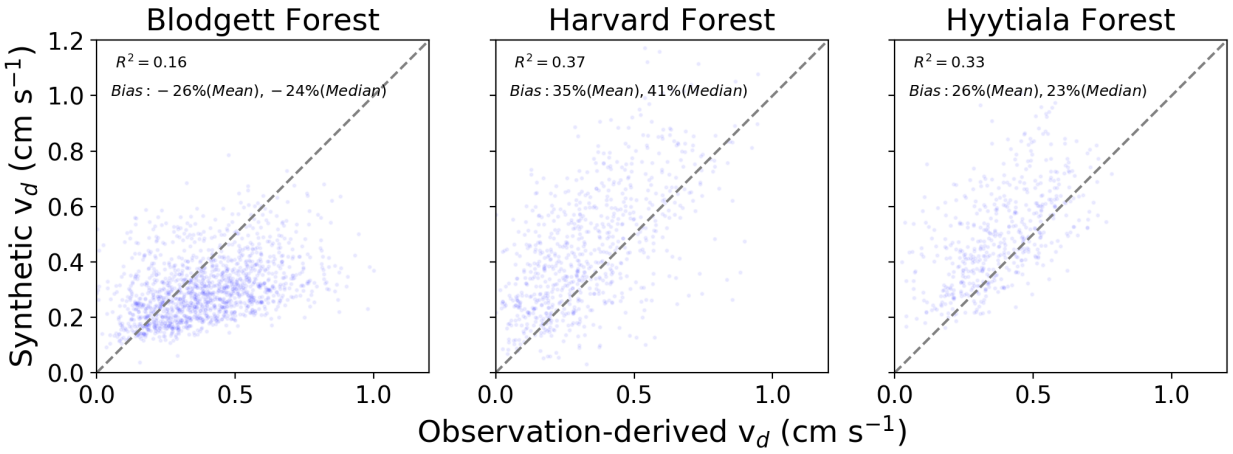

Figure S6. Synthetic and observation-derived daily daytime O_3 deposition velocity.

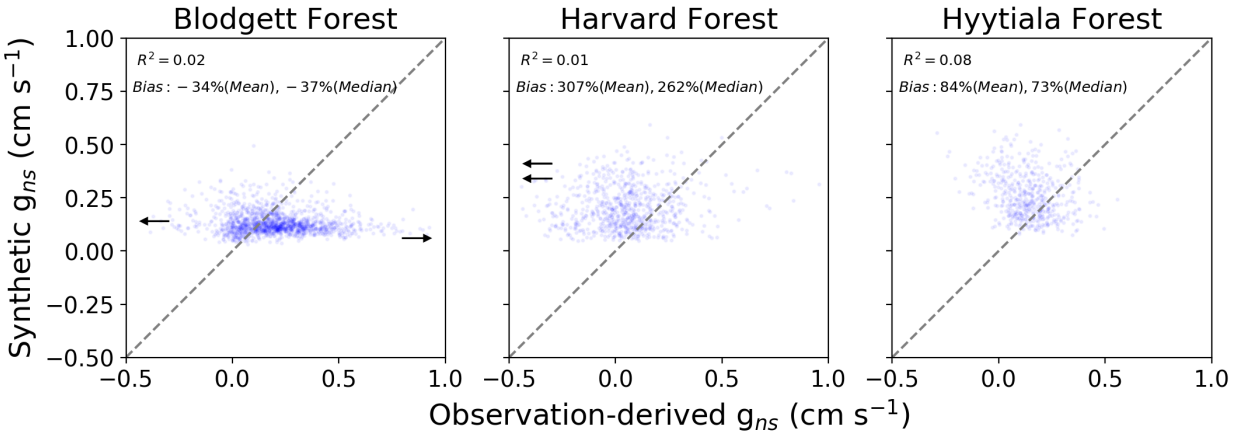

Figure S7. Synthetic and observation-derived daily daytime O_3 non-stomatal conductance.

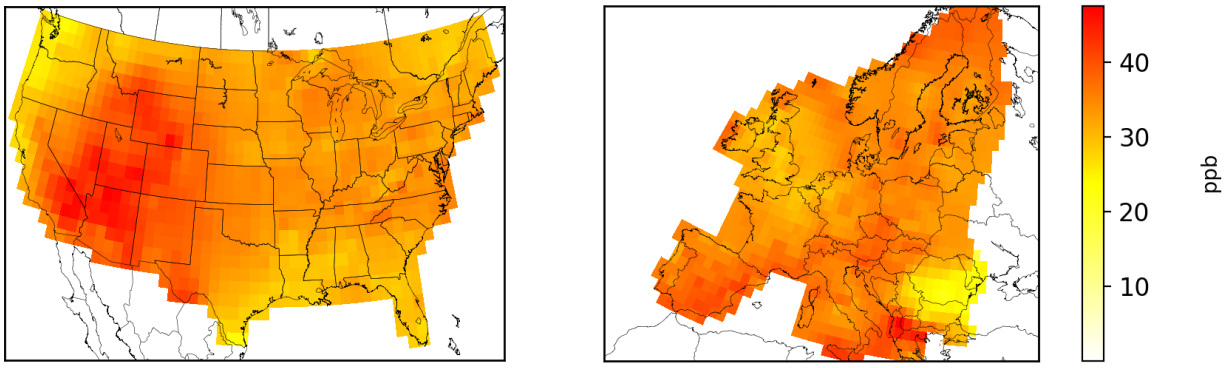

Figure S8. Mean daytime (8:00am-8:00pm local) O_3 concentrations for the US and Europe during the growing season (typically April-September) for 2000-2014. Data from Schnell et al. (2014).

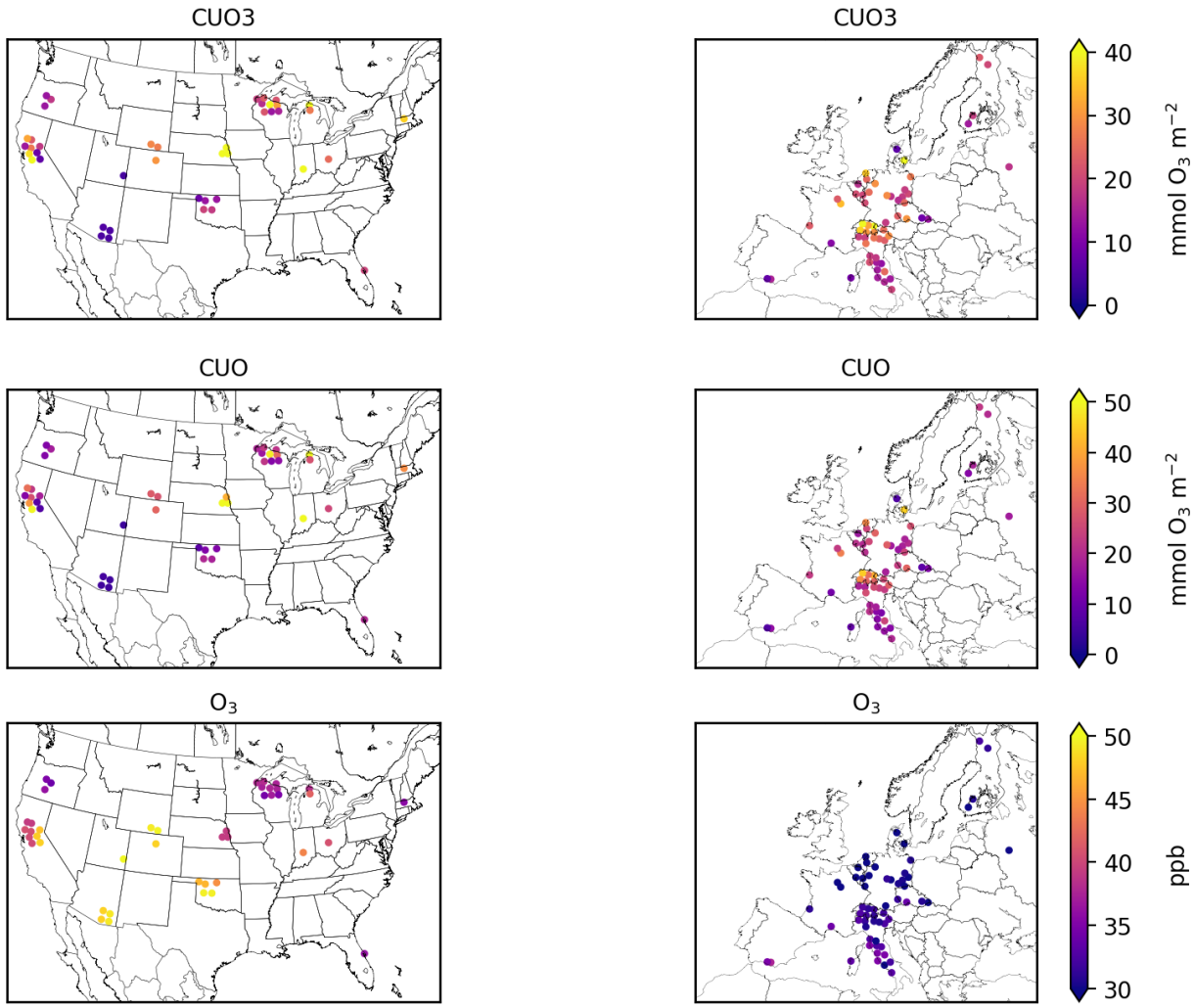
CUO3
CUO3
40
30
20
10
0
mmol O3 m−2
CUO
CUO
50
40
30
20
10
0
mmol O3 m−2
O3
O3
50
45
40
35
30
ppb

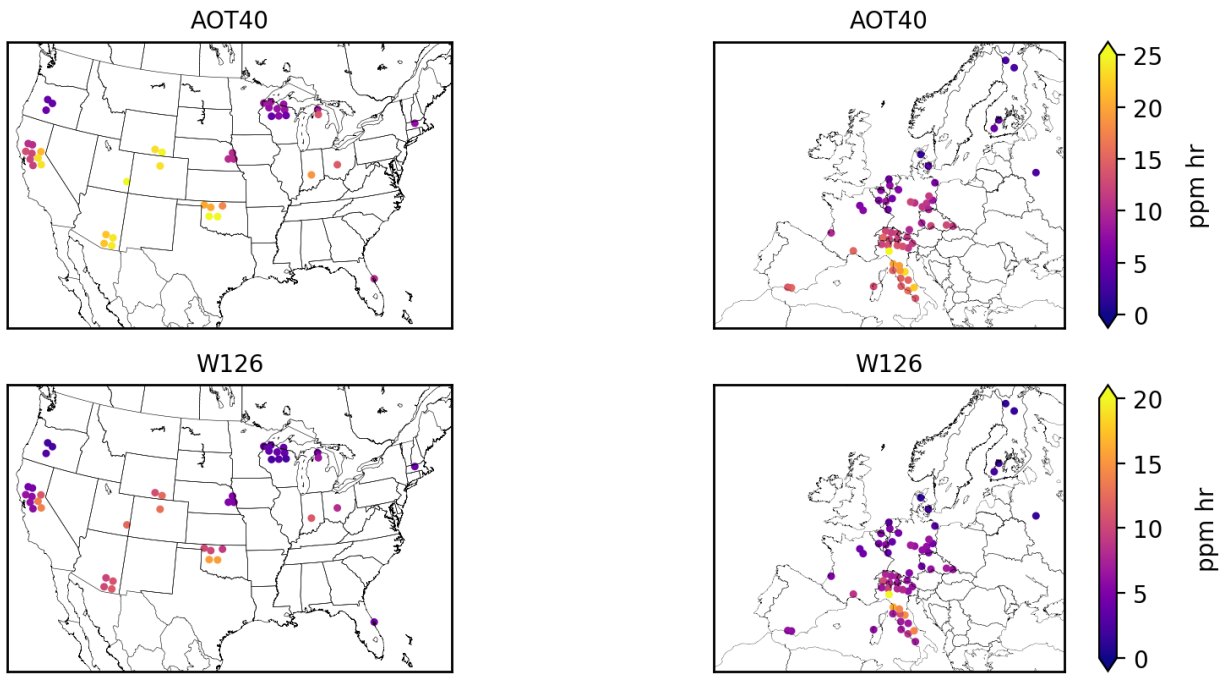

Figure S9. Metrics of plant exposure to O_3 at FLUXNET2015 sites in the US and Europe: CUO_3, CUO, mean O_3, AOT40, and W126. See Sect. 3.4 for metric definitions.